UCRL-19208

eg. 2

$\pi^{\pm}$-α SCATTERING AND THE PION FORM FACTOR

Anthony Fainberg
(Ph. D. Thesis)

April 2, 1969

AEC Contract No. W-7405-eng-48

LAWRENCE RADIATION LABORATORY
UNIVERSITY of CALIFORNIA BERKELEY

UCRL-19208

eg. 2

3+

DISCLAIMER

Contents

I. Abstract 1

II. Introduction 2

III. Experimental Description 6

IV. Analysis 26

A. The Optical Potential Method 37

B. The Phase-shift Method 51

C. Distortion Amplitudes by Other Methods. 55

D. Discussion 58

V. Conclusion 61

VI. Acknowledgements 62

VII. Appendix 64

VIII. Footnotes and References 65

IX. Figure Captions. 68

$\pi^{\pm}$-α Scattering and the Pion Form Factor

Anthony Fainberg

Lawrence Radiation Laboratory
University of California
Berkeley, California

April 2, 1969

ABSTRACT

A measurement of the $\pi^{\pm}$ He^4 scattering has been made at 53, 60, 68, and 75 MeV incident pion lab energy. The resulting differential cross sections are presented. An attempt has been made to extract the pion electromagnetic form factor using the difference in the π^+ and π^- cross sections which is sensitive to the coulomb contribution to the total scattering amplitude.

An optical model potential was postulated for the nuclear part of the interaction. Various different methods have been used to extract the form factor, with a view to minimizing model dependence. The most detailed model available, using a method of analysis designed to reduce this dependence gives R = 2.96±0.43F. Possible uncertainties in the model and its application are also discussed.

INTRODUCTION

Since nucleons possess pion clouds about themselves which determine, among other things, their electromagnetic structure, the structure of nucleons depends on the pion cloud and the structure of the pion, which possesses its own cloud. Frazer and Fulco[1] were able to make electron scattering data agree with the spectral representation method of treating nucleon structure by assuming a strong enhancement in the pion-pion system. This enhancement, subsequently discovered as the ρ resonance has a spin-parity 1^- permitting it to couple directly with a photon. Thus the pion can couple electromagnetically through exchange of a ρ. F_π is then expected to be proportional to $\frac{1}{1-q^2/m_\rho^2}$ where m_ρ is the ρ mass. This gives rise to a root-mean-square pion radius of 0.63F. A direct measurement of the pion form factor is then needed to test the theory of vector meson dominance.

One method of measuring this quantity was proposed by Hofstadter and Sternheim[2]. They suggested measuring the differential cross section for elastic pion-alpha scattering using both positive and negative pions. The argument is that the difference in the cross sections of the two reactions is sensitive to the coulomb amplitude since the strong interaction part of the interaction cancels to firstorder. This happens because the alpha is an isoscalar, and there is only one strongamplitude to determine. One finds then that $\frac{d\sigma^-}{d\Omega} - \frac{d\sigma^+}{d\Omega} = -4 \text{ Re } f^{s*} f^{coul}$ where f^s is the strong amplitude and f^{coul} is the Coulomb amplitude. In this experiment, the quantity examined is the difference divided by the average.

The first experiment along this line was performed by Nordberg and Kinsey[3], using 24-MeV pions, and a result of $R_\pi = 1.8 \pm 0.8$F. was obtained.

However in analyzing their data, they assumed a Coulomb amplitude which was just the Born Coulomb amplitude multiplied by the electromagnetic form factor of the pion-alpha system. However, Schiff pointed out[4] that an expansion of the matrix element for the interaction showed that distortion terms linear in the pion charge were present and could be significant. The matrix element for the interaction is written

$$T_{fi} = (\phi_f^-, U\chi_o) + (\phi_f^-, V\psi_o^+)$$

after Goldberger and Watson[5], with ϕ_f^- the outgoing wave function for nuclear interaction alone, χ_o a plane wave, ψ_o^+ the incoming wave function with nuclear and Coulomb interaction, U the nuclear potential and V the Coulomb potential.

The second term, which contains the Coulomb interaction, can be approximated by $(\phi_f^-, V\phi_o^+)$ where ϕ_o^+ is the incoming nuclear wave function, and Schiff showed this quantity to be proportional to

$$\Sigma(2\ell+1)\ P_\ell\ (\cos\ \theta)\ \int_o^\infty V(r)\ e^{2i\delta_\ell}\ R_\ell^2\ (r)\ dr$$

with δ_ℓ the nuclear phase shift and R_ℓ the nuclear radial wave function. This latter expression can be set equal to

$$\int_o^\infty V(r) j_o(qr) r^2 dr + \Sigma(2\ell + 1) P_\ell(\cos\ \theta) \int_o^\infty V(r)\ [e^{2i\delta_\ell}\ R_\ell^2(r) - j_\ell^2(kr)\ ] r^2 dr$$

with $q = 2\ k\ \sin^2\ \theta/2$ by adding and subtracting the j_ℓ^2 terms and performing the sum for the first term in the expression. This term is purely Coulomb and the second term is the distortion term effectively caused by the interference of the nuclear interaction upon the Coulomb amplitude Both are divergent at the upper limit, but West[6] has

rederived the amplitudes avoiding the divergency, giving a direct integral expression for the distortion term (see part D of the analysis). On the other hand, Auerbach et al.[7] use numerical techniques (see Appendix) to calculate the distortion term. Both methods modify the results of Nordberg and Kinsey to $R_\pi < 2.0F$ (2 standard deviations). Block[8] uses a technique slightly different from Wests's to calculate the distortion term and finds $R_\pi < 0.9F$(2s.d.).

In analyzing his own data at several energies from a helium bubble chamber, Block et al.[9] find $R_\pi < 0.9F$.(1s.d.) or $< 2.1F$.(2s.d.). Auerbach et al.[7] have presented a detailed discussion of the optical model as applied to the problem. To perform the analysis, one must postulate a form for the strong part of the interaction. Auerbach's method is to use a Kisslinger type optical model potential for the strong interaction. The Klein-Gordon equation can then be solved numerically, and, in addition to finding the size of the pion, one measures the optical parameters for the pion-alpha interaction. This model has been used in the analysis of the experiment presented here.

Berman[10] and others have criticized the interpretation of the experiment especially with regard to the existence of certain model-dependent distortion effects which are neglected in this analysis. These effects arise from the fact that the amplitude for this process contains contributions from relativistic effects which have not, to our knowledge, been calculated (see part D of analysis).

Our analysis gives $R_\pi = 2.96 \pm 0.43F$. Two other experimental techniques have been used in attempts to measure R_π.

The most direct method is the scattering of pions off atomic electrons. The divergence of the form factor from $F_\pi(q^2) \equiv 1$ is then a measure of the pion radius. This method is limited by the small value of momentum transfer available using present pion beam energies. Since, for a pion-electron system the center of mass is nearly the rest frame of the pion, the momentum transfer is small unless very high energies are used. In fact, at an incident lab energy of 30 GeV, the maximum momentum transfer available (backwards scattering) is only about .5 F^{-2}. In the pion electron scattering experiment, the momentum transfer goes roughly as the square root of the incident energy, 300 GeV gives about $1.9F^{-2}$. If the density is taken to be a Gaussian, a square well, or a Saxon-Woods the first order term in the expansion of the form factor is $q^2 r_\pi^2/6$. Low q^2 then implies lack of sensitivity to r_π. If the pion has, say, the vector dominance model predicition for the rms radius (0.63F.), the deviation of the pion electromagnetic formfactor from one would be about .03 for the 30 GeV case and about .13 for 300 GeV. Cassel et al. have made the measurement[11] and were able to assign a limit of $R_\pi < 3.0F$. The 300 GeV case is promising and should be tried when such pion energies are available.

Another possible method is pion electroproduction. In the reaction $e + p \rightarrow e + n + \pi^+$, one assumes a single photon exchange between the electron and the strongly interacting system. Then, one has the photoproduction of a pion by a space-like photon which is polarized both transversely and longitudinally. The pion form factor arises only from the pion pole diagram which has a maximum

effect when the pion-production angle is closest to the pole. This is along the direction of the virtual photon, or equivalently, of the 3 momentum transfer of the electron. A transverse photon cannot knock a pion directly forward because of its helicity, so the contribution to the pion-pole amplitude is from longitudinal protons. The experiment is performed at different polarizations for the same momentum transfer and energy to estimate the longitudinal contribution, and then at different momentum transfers to get the effect of the pion size. The kinematics are thus arranged to maximize the effect of the pion pole at the pion vertex, Zagury[12] has developed a relativisitic formalism for treating this reaction using dispersion relations in which the differential cross section can be expressed with F_π as a free parameter. There is some uncertainty about the model-independence of the theory, but two experiments have been carried out with the reported error including this uncertainty. Akerlof et al. find $R_\pi = 0.80 \pm 0.10$ F.[13] and Mistretta et al. find $R_\pi = 0.86 \pm 0.14$ F.[14] The momentum transfer in these experiments is typically between 1. and 15. F^{-2}.

Experimental Description

A pion beam of 90 MeV obtained from an internal target of the 184-inch Berkeley Synchrocyclotron is shown schematically in Fig. 1. Negative pions produced in the forward direction at the target were accepted by the transport system. Positive pions (produced in the backward direction) were obtained in the same beam line by reversing the cyclotron main field. Consideration of sensitivity to the pion form factor leads to an optimum energy for the measurement of about 60 MeV for the incident pions;[15] here (at the minimum in the nuclear

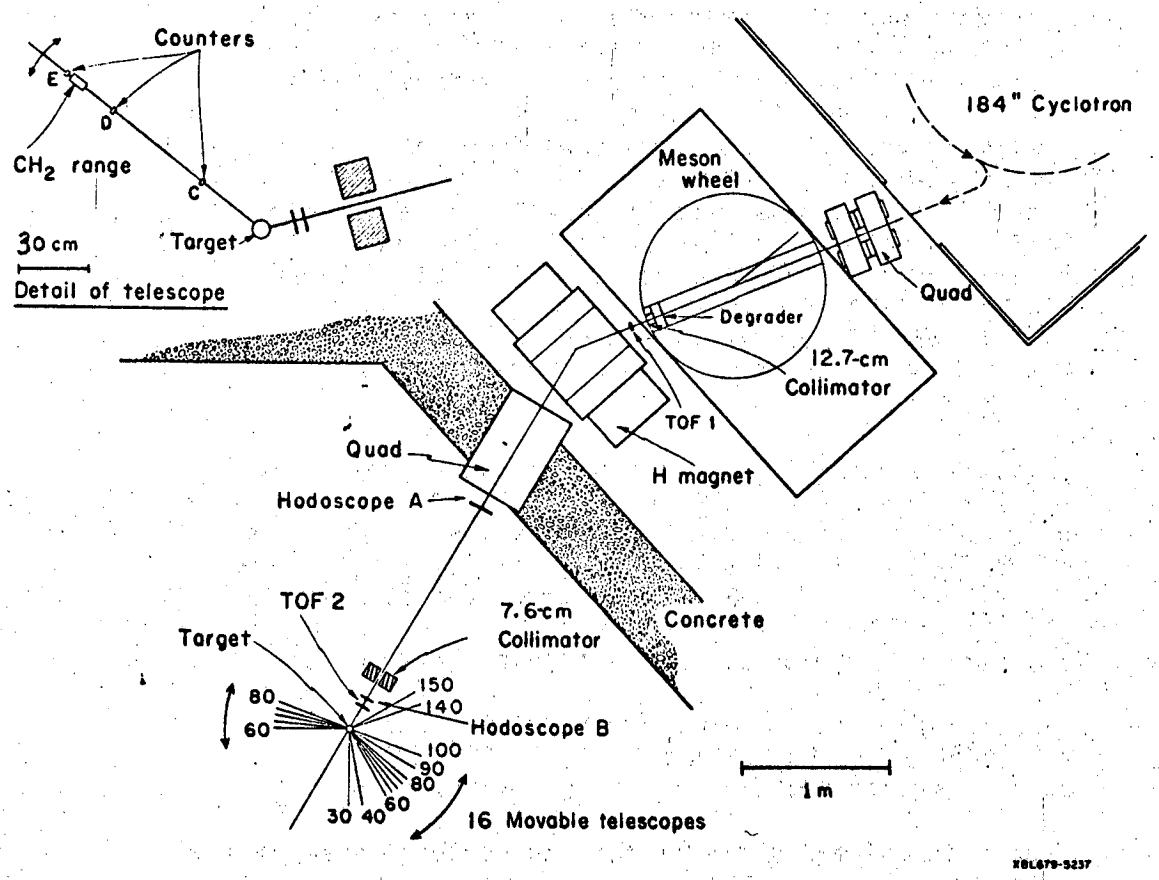
Counters
E
D
C
CH_2 range
30 cm
Target
Detail of telescope
184" Cyclotron
Meson wheel
Degrader
Quad
12.7-cm Collimator
TOF 1
H magnet
Quad
Hodoscope A
TOF 2
Target
7.6-cm Collimator
Concrete
80
60
150
140
Hodoscope B
100
90
80
60
30 40
16 Movable telescopes
1 m
XBL679-5237

Figure 1

cross section) a sufficiently large value of momentum transfer is obtained and the interference between the Coulomb and nuclear amplitudes is significant. The beam was degraded at an intermediate focus before the bending magnet instead of immediately before the target so that the target distribution could easily be determined from the hodoscopes, and so that the momentum bite would be small. The momentum band of ±3% was essentially the same for all energies.

Time-of-flight counters (labelled TOF 1 and TOF 2) were used to reject electrons or positrons in the beam (about 25% for electrons and 5% for positrons) that would otherwise introduce an asymmetry in the beam normalization. The time resolution was set to include the muons from pion decay, which were approximately 15% of the flux; the correction for muons is described below. The direction of the incident pion in the horizontal plane and the spatial distribution of pions at the target were defined by hodoscope A (11 counters, 1.9 cm wide, 0.63 cm thick) and B (5 counters, 1.9 cm wide, 0.63 cm thick). Two further beam-defining counters were used for calibration purposes. A lead opening 10 cm long was situated about 30 cm from the target with a 7.6 x 7.6-cm aperture to reduce the flux of particles incident on the walls of the target and the vacuum jacket. The target itself consisted of a 7.6-cm-diameter vertical cylinder of liquid helium.

Scattered pions were detected in an array of 16 doped polystyrene scintillation counter telescopes each consisting of three counters placed respectively 30.5, 86.4 and 101.7 cm from the target, as shown in Fig. 1. The nearest to the target is called the C counter, the

next is the D, and the final counter is the E. These telescopes were mounted in such a way that they could be rotated about the target; this facility allowed each telescope to be set in the primary beam for efficiency measurement. Also each telescope could be used to make measurements at several angles. The most interesting region, from 60 to 80 deg., was covered by 10 of the telescopes, 5 on either side of the beam. The remainder spanned the other angles between 30 and 150 deg. The dimensions of the counters were 2.54 c.m wide, 1.27 cm thick, and either 30.5 or 50.8 cm long, the longer type covering the angular interval 60 to 100 deg., where the contributions to the angular resolution due to the length of the counters is small.

Two contaminants among the scattered particles were inelastically scattered pions, and protons arising from pion capture. The inelastic pions were rejected by a range requirement in the telescopes. At each angle, range curves were obtained and sufficient range (consisting of slabs of CH_2) was inserted to reject the inelastic pions, which have at least 20 MeV less energy than those elastically scattered. A typical range curve is shown in Fig. 2, with the range indicated for 20 MeV below elastic scattering.

The trigger for an event was a beam-particle trigger plus a scattered-particle trigger. The former was defined by a time-of-flight within the appropriate gate as well as by the two hodoscopes; the latter required all three telescope counters.

In order to reduce the number of logical circuits, we mixed signals from the counters in three telescopes in each fast-logic bin (F-bin).

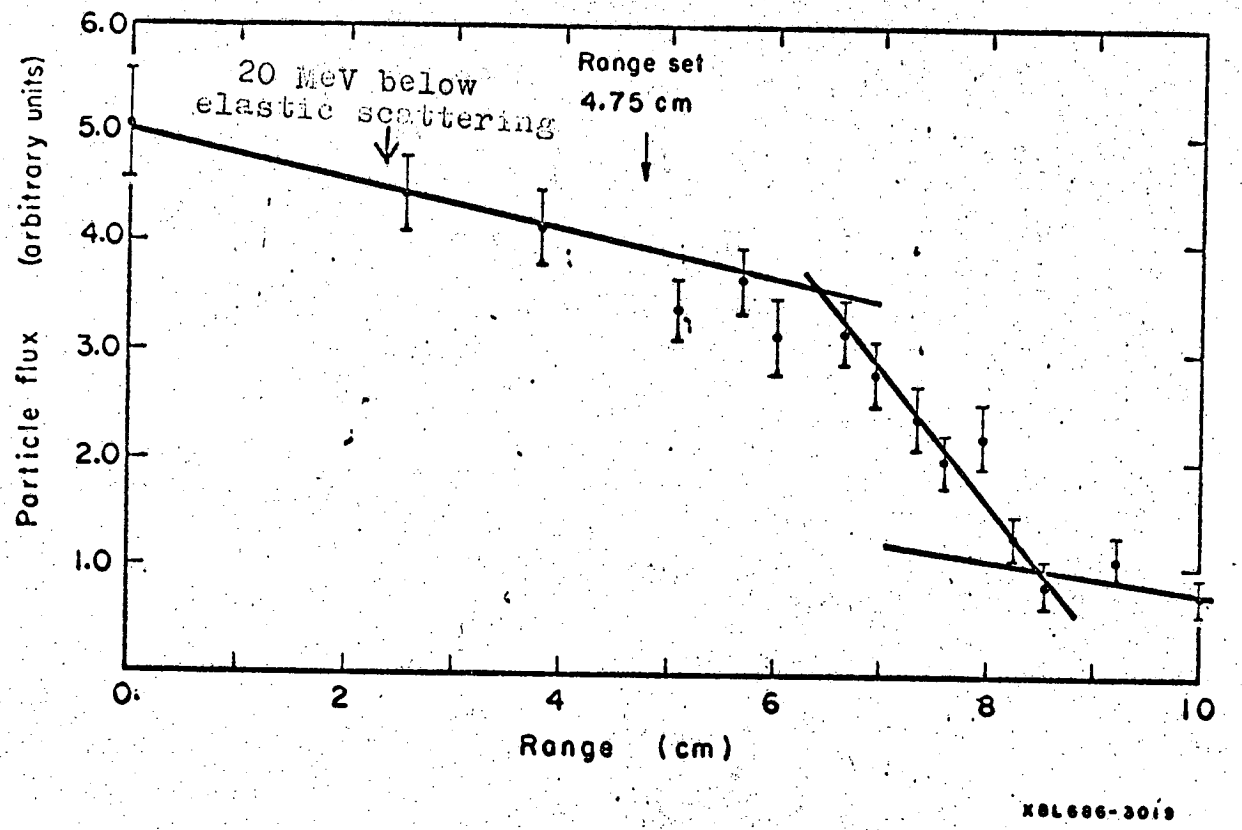
6.0
5.0
4.0
3.0
2.0
1.0
0
2
4
6
8
10
Particle flux (arbitrary units)
Range (cm)
20 MeV below
elastic scattering
Range set
4.75 cm
XBL686-3019

Figure 2

These telescopes are physically far apart so that a trigger from the F-bin, which consists of at least one each of a C, D, and E counter, will probably not correspond to a physical particle unless all three of the counters which fire are in the same telescope. In practice, about 90% of the triggers corresponded to real particles, and the rest were accidental which were eliminated by the data analysis computer program.

As soon as a trigger (i.e. the beam telescope plus a trigger from the F-bin) reaches the Master Gate Generator, (see Fig. 3) an inhibit signal prevents further information from passing beyond this point. Signals are also sent to the F-bins setting bistable flip-flops of the counters which have fired for the event. The discriminators, which receive signals directly from the counters of the beam and scattering telescopes are also gated off, while the on-line computer obtains the information of the event. The flip-flops in the F-bins are read by the computer and reset. After the computer has finished, all gates are reopened, and the equipment is ready for taking further data.

Protons are rejected by use of pulse-height information as follows. Information on which of the counters fired for any one event in the telescope and hodoscope arrays is stored in the on-line computer, and on tape for subsequent analysis on a large off-line computer.

The pulse heights of all the C counters are mixed and sent, when there is an event trigger, to an anlaog to digital converter (ADC). This pulse height is read by the computer. The separation of pions and protons is essential, since the protons from the capture process, if counted to any significant extent, could introduce a marked asymmetry

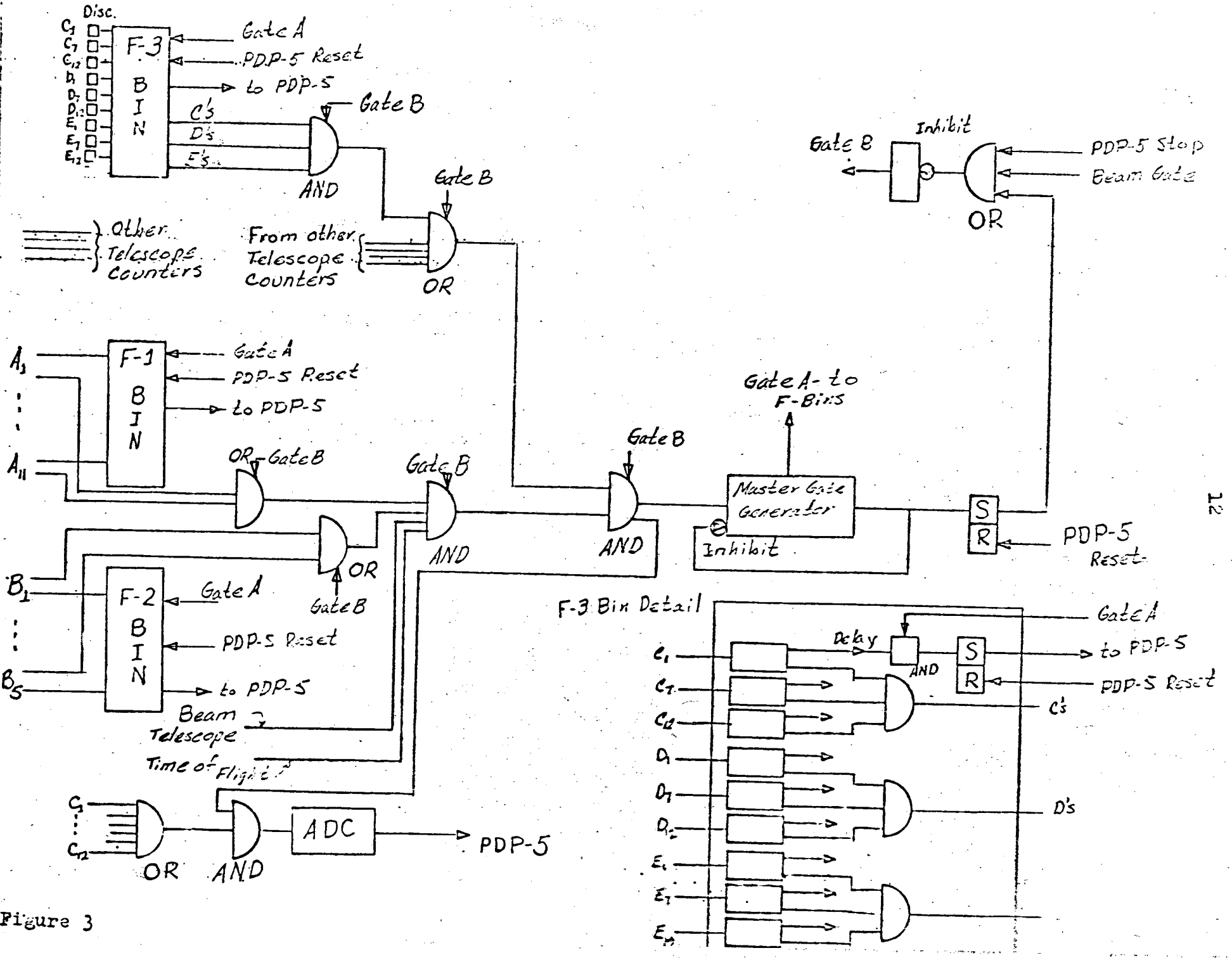
Disc.
F-3
B I N
Gate A
PDP-5 Reset
to PDP-5
C's
D's
E's
Gate B
AND
Other Telescope Counters
From other Telescope Counters
Gate B
OR
Gate B
Inhibit
PDP-5 Stop
Beam Gate
OR
F-1
B I N
Gate A
PDP-5 Reset
to PDP-5
OR-Gate B
Gate B
Gate B
AND
AND
Gate A- to F-Bins
Master Gate Generator
Inhibit
S
R
PDP-5 Reset
OR
Gate B
F-2
B I N
Gate A
PDP-5 Reset
to PDP-5
Beam Telescope
Time of Flight
F-3 Bin Detail
Delay
AND
S
R
Gate A
to PDP-5
PDP-5 Reset
C's
D's
OR
AND
ADC
PDP-5

Figure 3

between π^- and π^+ cross sections. The probability of capture of a pion in nuclear matter on two unlike nucleons is several times that for which gives rise to an observed ration of energetic proton yields from helium of about 18 to 1 for π^+ and π^- capture respectively. To allow for the slight overlap of the pulse-height spectra for each telescope, each run was fitted by an expression which was the sum of two Gaussian distributions; the total area under the peaks was constrained to be the total number of counts in that telescope, but the ratios of the areas of the peaks, their position, and their widths were allowed to be free parameters. Examples of pulse-height spectra are shown in Fig. 4.

A measurement of pulse height was made in the beam to assure that a Gaussian form is adequate to fit the distribution in the counters. The result is shown in Fig. 5.

During the runs, many checks on the consistent behavior of the counters, on the electronics, and on the pion beam itself were made. Most of these checks were monitored by the on-line computer. The important accidental coincidence rates were also monitored.

Checks on the efficiency of each telescope were made by rotating each into the primary beam (0-deg direction) and measuring the ratio of telescope counts which were registered in the computer triggered by a coincidence between three additional counters, to the number of coincidences between the three additional counters--these coincidences defined a pion as having passed through all three telescope counters.

The method of running was typically to spend about 1 hour with the

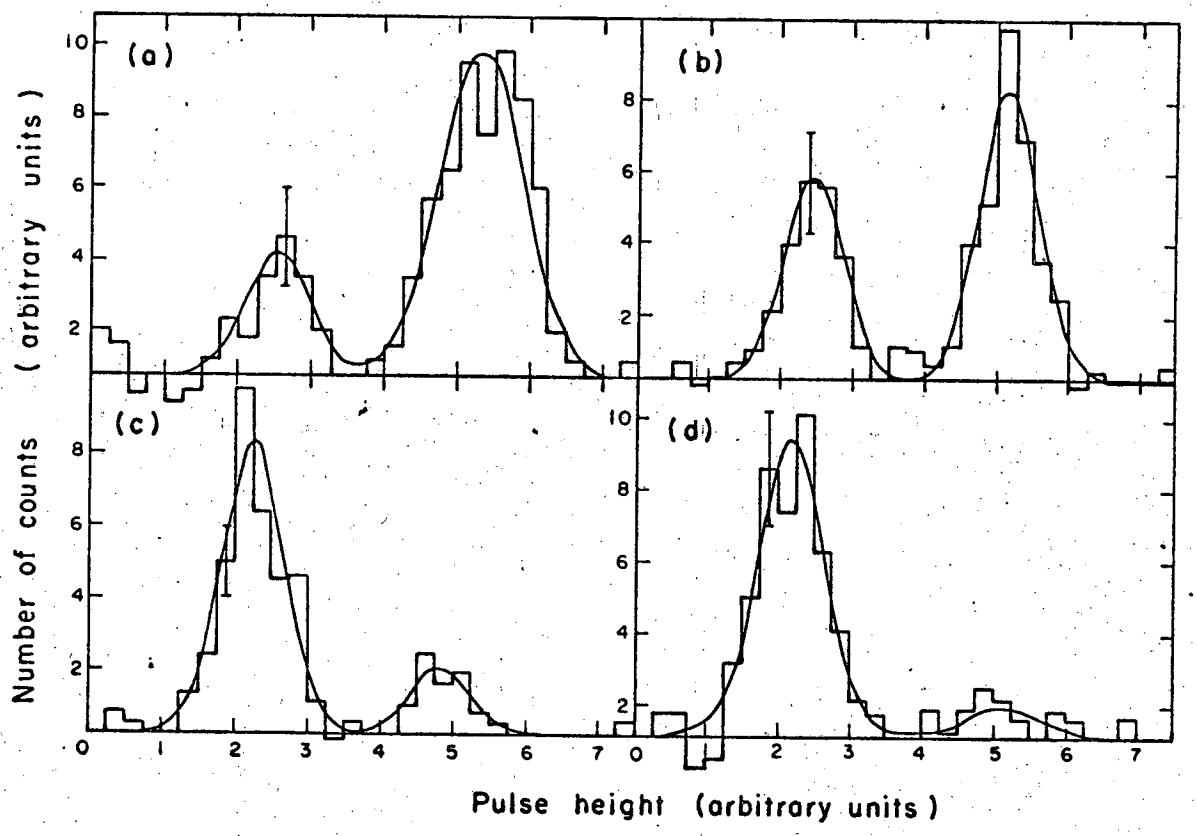
(a)
(b)
(c)
(d)
Number of counts (arbitrary units)
Pulse height (arbitrary units)
XBL686-3012

Figure 4

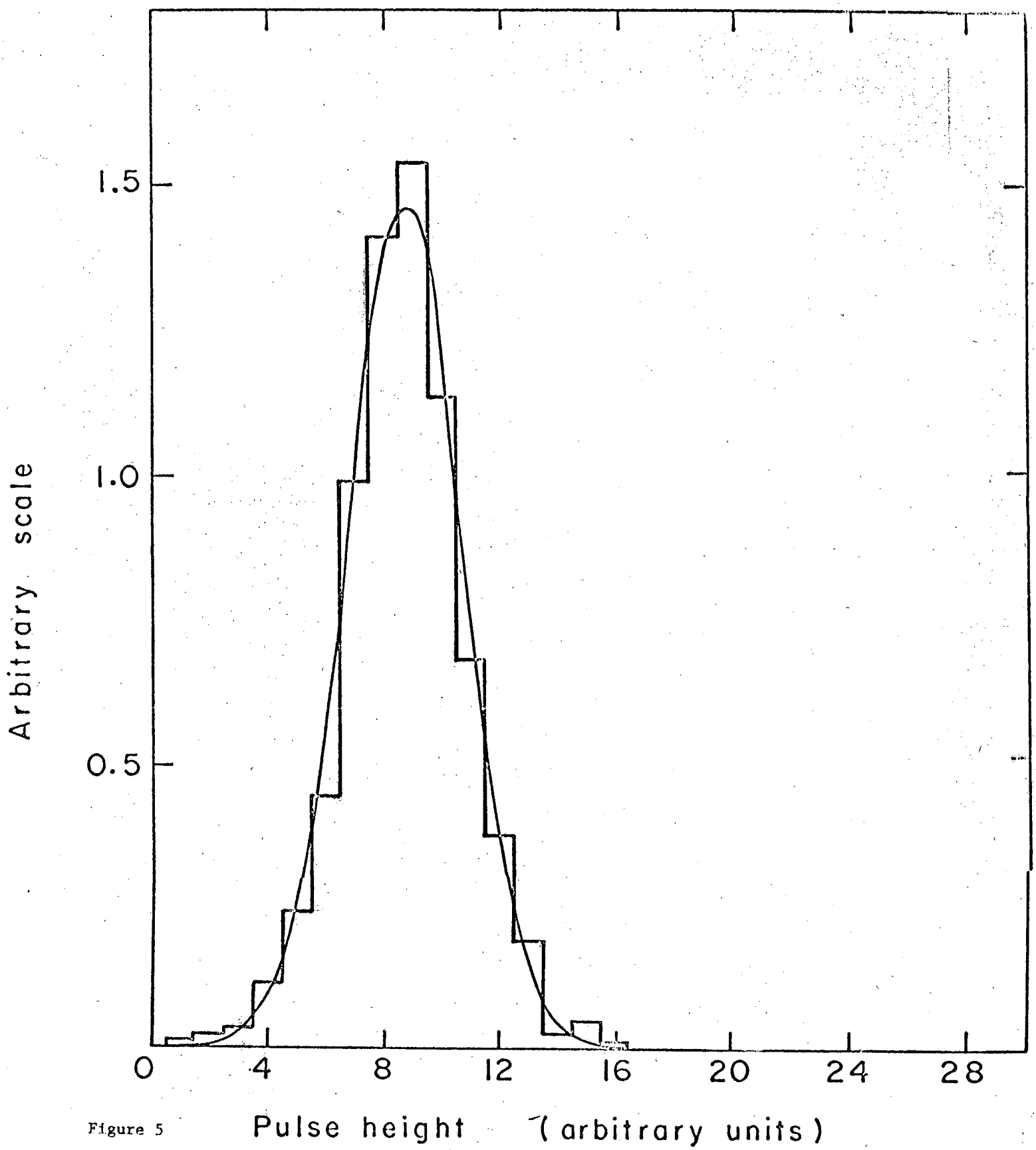
1.5
1.0
0.5
Arbitrary scale
0
4
8
12
16
20
24
28
Pulse height (arbitrary units)

Figure 5

target full (about 10^4 events) and then 0.5 hour with the target empty, followed by about 5 minutes triggering the computer only on a beam particle; this last type of run provided a random sample for measuring the angular and spatial distribution of the beam at the target as well as a monitor on the probability of random counts in the telescope counters. The signal-to-background ratio was typically 10:1 at forward and backward angles and about 2:1 around the minimum in the cross section.

Several corrections were applied to the data, both to the number of scattered pions at a given angle and to the intensity of the incident beam. The important ones are summarized in Table I, and all are discussed below. It should be noted that several of the corrections are the same for both the positive and negative cross-section measurements.

The formula used for the differential cross section is:

$$\frac{d\sigma}{d\Omega} = \frac{N/D \times 10^{-7} \times (1-N_{mu}) \quad (1+R_{abs})}{N_\pi \times t_p \times \Omega \times \ell \times N_{mc}} \frac{1}{t_{gt}} \quad \cdot(1+R_{nd})\cdot(1-M_{inel})$$

The quantities used in the above formula are as follows:
N is the number of pion counted in a given telescope $D \times 10^7$ is the number of scaled counts in the beam telescope N_π is the fraction of pions in the beam. t_p is the number of target particles per cm^3 of target $\Omega \times \ell$ is the average solid angle subtended by a point in the target multiplied by the average target length. N_{mc} is the multiple scattering correction calculated by a Monte Carlo program. N_{mu} is the muon correction from the decay of elastic pions R_{abs} is the fraction of

Table I. Corrections applied to the : data.

Description of measurement or correction	Source of estimate	Approximate amount of correction (%)	Approximate error in measurement or correction (%)
CORRECTIONS TO AND MEASUREMENTS OF BEAM INTENSITY:			
1. Number of beam particles	Scaled at 100 mHz	---[a]	
2. μ fraction	(i) Monte Carlo (ii) Range + time-of-flight measurements	-15	3
3. Randoms	Measured experimentally	3	1.5
4. Dead time	Measured experimentally	< 1	
CORRECTIONS TO AND MEASUREMENTS OF NUMBER OF PIONS SCATTERED:			
1. Number of pions	Scaled	---	2 (statistical)
2. Solid-angle measurement	From counter position survey	---	1.0
3. Multiple scattering in target + counters + range	Monte Carlo	+10	±1.5
4. π-μ decay		+15	
5. μ's detected from π-μ decay		- 5	
6. Nuclear absorption and scattering in counters and range	(i) $\sigma_{inelastic}$ and $\sigma_{elastic}$ data (ii) measurements in beam	+ 7[a]	2 (exptl. errors)
7. μ's Coulomb scattering in ^{4}He	Calculated	2 at forward angles[a]	<0.5
8. Inefficiency of counters	Measured frequently during expt.	<1	<0.5
9. Contamination by protons from π capture	Distinguished by pulse height	---	---
10. Correction due to two C counters firing	From "beam triggered" runs	1 to 2[a]	<0.5

a. Cancels for D/A.

scattered pions which are absorbed by the counters or by the range. T_{gt} is the loss of beam due to geometry. R_{nd} is the random and dead times correction. M_{inel} is the correction for muons from inelastic decay.

We now explain in detail each correction.

A Monte-Carlo-type program was used to calculate multiple scattering and muon decay corrections to the number of counts scaled in a telescope. The program took into account scattering by the range, the counters and the materials in the target walls. The angle of scattering was taken to follow Gaussian distribution. It was found that the more accurate Moliere distribution did not affect the results. The projected rms angle was taken to be $\Theta_{rms} = 15/(pv)\sqrt{L/L_{rad}}(1+\epsilon)$ (with p and v in MeV units, L the length in cm and L_{rad} the radiation length) after Barkas and Rosenfeld[16]. Barkas and Rosenfeld[18] and Rosenfeld et al.[17] also give values for L_{rad} and ϵ which were used. In the program, pions were generated at randomly selected points in the target and aimed at the first counter in the telescope. The points chosen were weighted by the vertical beam distribution. The horizontal distribution was found to have no effect and was not used. They are permitted to decay in flight at the appropriate rate. The number of pions reaching the final counter divided by the number which could have reached it had there been no counters or range or decay was the correction factor N_{mc}. In the same program, we counted the number of muons which reached the final counter, leading to N_{mu} which was the number of muons counted divided by the same normalization factor

as the N_{mc}. This program was run for each angle used in the experiment and for hydrogen and helium separately(hydrogen used no range). For each of the two targets, a polynomial fit was made to the correction function N_{mc} as a function of angle. This factor varied fairly strongly with angle, whereas N_{mu} did not. Each point gave errors of 2-3 per cent and by fitting with a smooth polynomial curve, we reduced the statistical fluctuations from point to point.

The main correction to the incident beam intensity was for the muon contamination (N_{π}). This was calculated by using a Monte Carlo type program simulating the transport of pions from the cyclotron internal target to the helium target and including π-μ decay in flight. The predicted range curves and time-of-flight spectra compared with those obtained experimentally and were found to be in good agreement. The fraction of muons varied from 20 ± 3% at 51 MeV to 12 ± 2% at 75 MeV.

The solid angle at the target subtended by the telescope is calculated by Crawford's formula (18) using $\Delta\Omega = \tan^{-1}\frac{ab}{cd}$ (see Fig. 6). Since $\Delta\Omega$ varied from point to point in the target, we integrated $\Delta\Omega$ over the target weighting it by the beam distribution. If g(y) is the normalized beam distribution in the horizontal plane, such that then the average solid angle multiplied by the average length traversed by the beam in the target is

$$\Delta\Omega x\ell = \int_{-3.81\,cm.}^{3.81\,cm.} \int_{3.81^2_{cm}-x^2}^{3.81^2_{cm}-x^2} g(y)\Delta\Omega(x,y)\, dydx \Big/ \int_{-3.81cm.}^{3.81cm.} dy$$

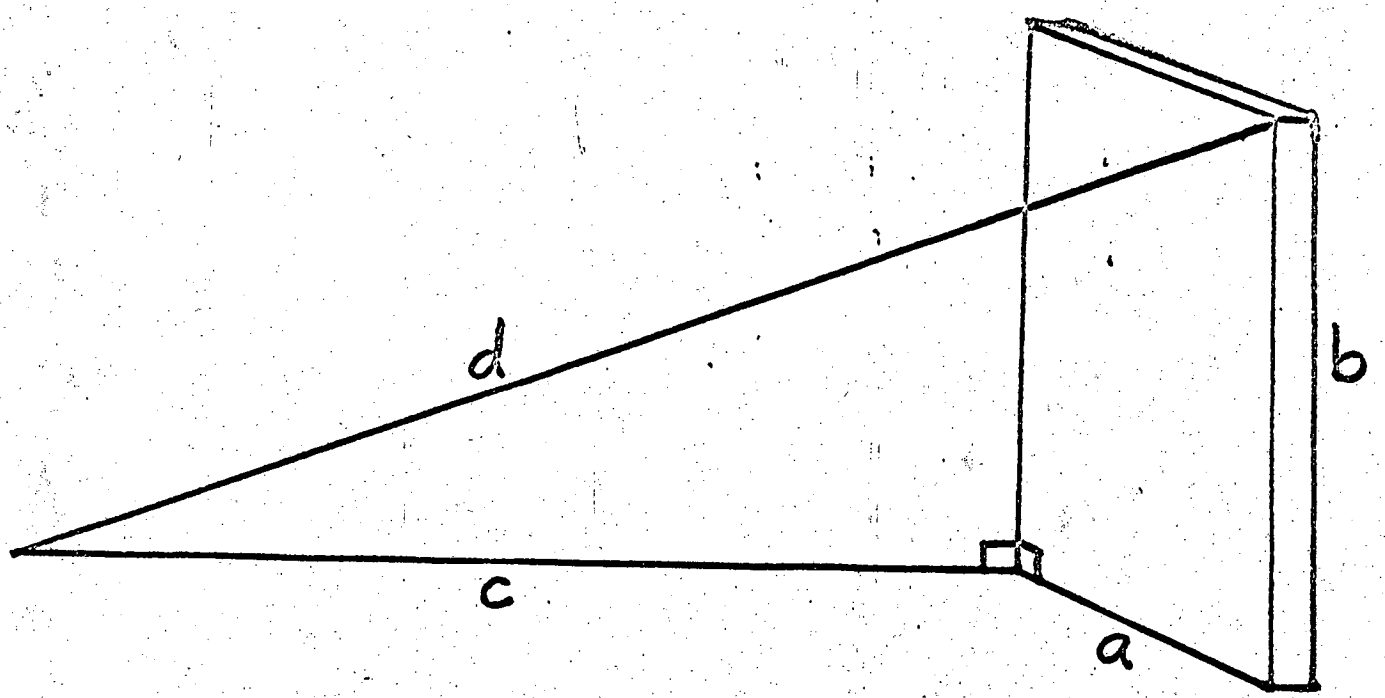

Figure 6(a)

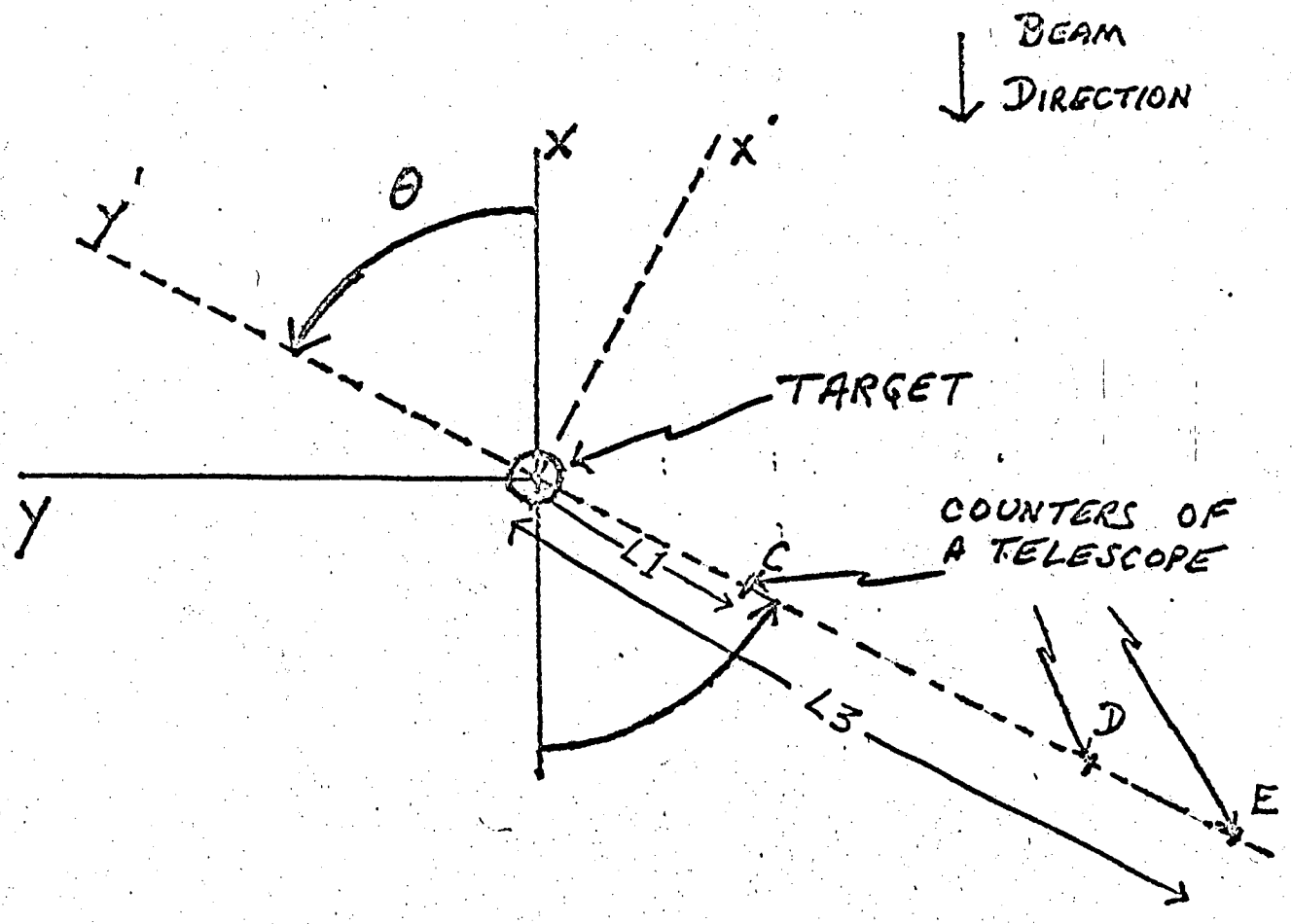
BEAM
DIRECTION
X
X'
Y'
θ
TARGET
Y
COUNTERS OF
A TELESCOPE
L1
C
L3
D
E

Figure 6(b)

$\Delta\Omega$ was calculated using Crawford's formula and found to be

$$\Delta\Omega_{|x'|\leq 1.27} = 2\left[\tan^{-1}\frac{H(1.27-x')}{(L3-y')\sqrt{(L3-y')^2+H^2+(1.27-x')^2}} - \tan^{-1}\frac{H(1.27+x')}{(L3-y')\sqrt{(L3-y')^2+H^2+(1.27+x')^2}}\right]$$

$$\Delta\Omega = 2\left[\tan^{-1}\frac{H(1.27+x')}{(L3-y')\sqrt{(L3-y')^2+H^2+(1.27+x')^2}} - \tan^{-1}\frac{H(x'-c)}{(L3-y')\sqrt{(L3-y')^2+H^2+(x-c)^2}}\right]$$

$|x'|\geq 1.27$, where $C=\frac{L3}{L1}(x'-1.27)$, H is 1/2 the height of the counter, L3 is distance of E counter from target, L1 is distance of C counter from target.

If Θ is the angle of the telescope with respect to the beam, then

$$x' = x\sin\Theta - y\cos\Theta$$

$$y' = x\cos\Theta + y\sin\Theta$$

The vertical beam distribution was centered about .95 cm above the median plane with a half-height of about 6.6 cm. For the short counter telescopes and for four of the long counters, the E counter was higher than the D in the vertical direction. For the other telescopes the D was higher. This resulted in a modification of the quantity $\Delta\Omega x\ell$. This correction factor and the product $\Delta\Omega x\ell$ are calculated by numerical integration for each telescope. The correction factor was less than 1% for all cases. The procedure used was to calculate $\Delta\Omega x\ell$ for all telescopes at 90 deg and then to apply an

angular correction (which arises from the non-uniform beam distribution in the horizontal plane) for each telescope and each angle. The solid angle factor was about 10% larger at 30 deg than it was at 90 deg and was symmetric about 90 deg.

The final correction to the solid angle was necessitated by the fact that in reality the counters were not perfectly aligned. These deviations were measured by a transit and led to corrections of the order of 3% of the solid angle.

A correction to the beam normalization due to the geometry had to be made. It was possible for a particle to pass through both hodoscopes, the time-of-flight counters and the beam telescope without hitting the target. This correction factor was calculated with a Monte-Carlo type program similar to that described above, since multiple scattering was included. This correction factor was about 11%, and is labelled t_{gt}.

There were three corrections due to randoms and dead time which must be made. Other random corrections are negligible.

1) Dead time losses in the scaling system.

Since the prescalers count at the rate of 100mHz, the dead time is taken to be 10ns. The probability of two particles arriving within this time has been measured by using the doubles rate in hodoscope B, which has a 20ns resolution. This rate will thus be twice the dead timeloss. It was found to be about 1% varying slightly with energy and signature.

2) Randoms between array A and the rest of the beam telescope.

The randoms for both correlated and uncorrelated particles were measured by delaying the signal from A by the length of one cyclotron r.f. pulse and finding the coincidence rate with the signal from the rest of the telescope. Then, one has a random rate which includes correlated and uncorrelated particles. The fraction of uncorrelated particles was calculated as follows. The ratio of the beam telescope rate to the rate of the beam telescope without the A array was measured. This gave the ratio of correlated particles to all particles

$$\frac{\text{Telescope with A}}{\text{Telescope without A}} = \frac{\text{Correlated}}{\text{Correlated + Uncorrelated}}$$

From this, the fraction of uncorrelated particles is just $1 - \frac{\text{T with A}}{\text{T without A}}$ Multiplying this by the randoms rate from delaying by an rf pulse, we get the real randoms rate. This rate was about 0.5%.

3) Randoms between the upstream time-of-flight counter and the rest of the beam telescope.

This was measured analogously to (2), The correction was about 35%. It was larger than (2) because of the more intense rate and because of the long distance between this counter and the rest of the beam telescope.

The randoms reduce the number of beam particles from the measured quantity and the dead time increases the number. The errors on these corrections are about 30% of their values. These corrections are lumped together in R_{nd}.

There are some muons from inelastic pion decay which pass through the range and are counted. The same Monte-Carlo type program is used to calculate this quantity which is M_{inel}. It is significant only in

the dip in the differential cross section (between 60 and 80 deg) and is about 1 or 2 per cent there.

Nuclear scattering and absorption were estimated by using the data of Stork[19] and Byfield[20] as well as data obtained in the beam in this experiment, both sources of information being essentially in agreement; the error of 2% in this correction is an estimate from the published data. This gave R_{abs}.

A correction needs to be made for the effect of two C counters firing during one event. This increases the pulse height for this event and makes it appear as a proton which is then rejected (see discussion on pion-proton discrimination). These corrections were made by counting the number of these doubles which occurred. The answer varied with energy and signature and was approximately 1% ± .25%.

Data for each sign of particle were obtained at 51, 60, 68, and 75 MeV. The correction for the protons arising from $\pi-$ capture was measured to be 5% at 60 MeV. The corrections at other momenta were made by assuming that the ratio of the proton yields from $\pi+$ and $\pi-$ capture is constant with energy.

This correction was included in the number N of pion counts in a telescope, as was the proton correction.

As a check on the whole setup, some data were obtained at 60 MeV, with hydrogen used in the target. For these measurements the absorbing ranges were removed from the telescopes. These data are shown in Fig. 7, compared with the predictions of the most recent πp phase-shift analysis.[21] The agreement is reasonable considering the precision, in

this region of the data upon which the phase-shift analysis is based (see the data at about 58 MeV of Bodansky, Sachs, and Steinberger with which our data is consistent)

Analysis

In this section, the data are presented and two methods for extracting the pion radius are described. The first depends on the optical model, using it to fit the data while letting the radius be a free parameter. The second relies primarily on a phase shift analysis to fit the data, utilizing the optical model only to calculate the distortion amplitude. Various other methods of calculating this amplitude are also discussed.

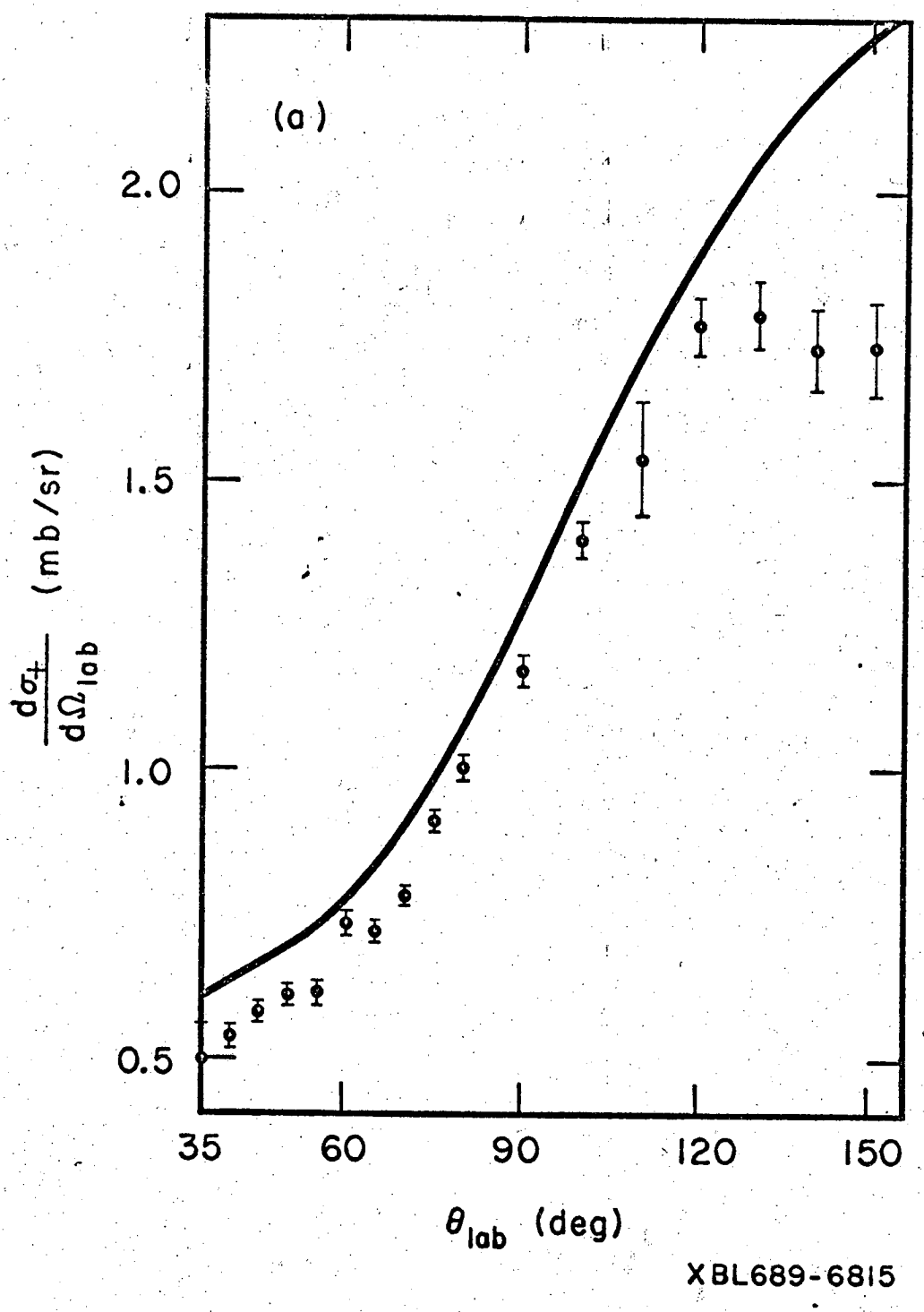
(a)
2.0
1.5
1.0
0.5
$\frac{d\sigma_+}{d\Omega_{lab}}$ (mb/sr)
35
60
90
120
150
θ_{lab} (deg)
XBL689-6815

Figure 7(a)

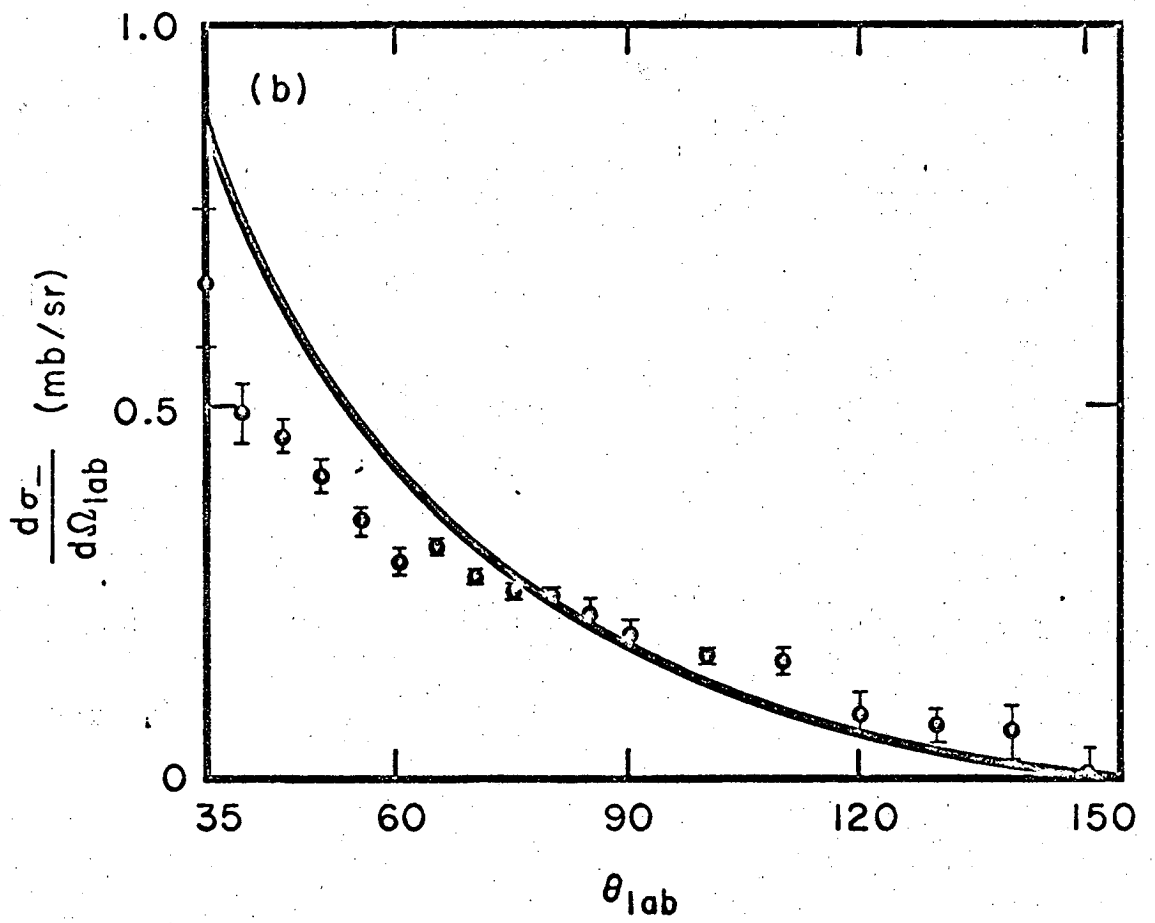
1.0
(b)
0.5
0
35
60
90
120
150
$\frac{d\sigma_-}{d\Omega_{lab}}$ (mb/sr)
θ_{lab}
XBL689-6816

Figure 7(b)

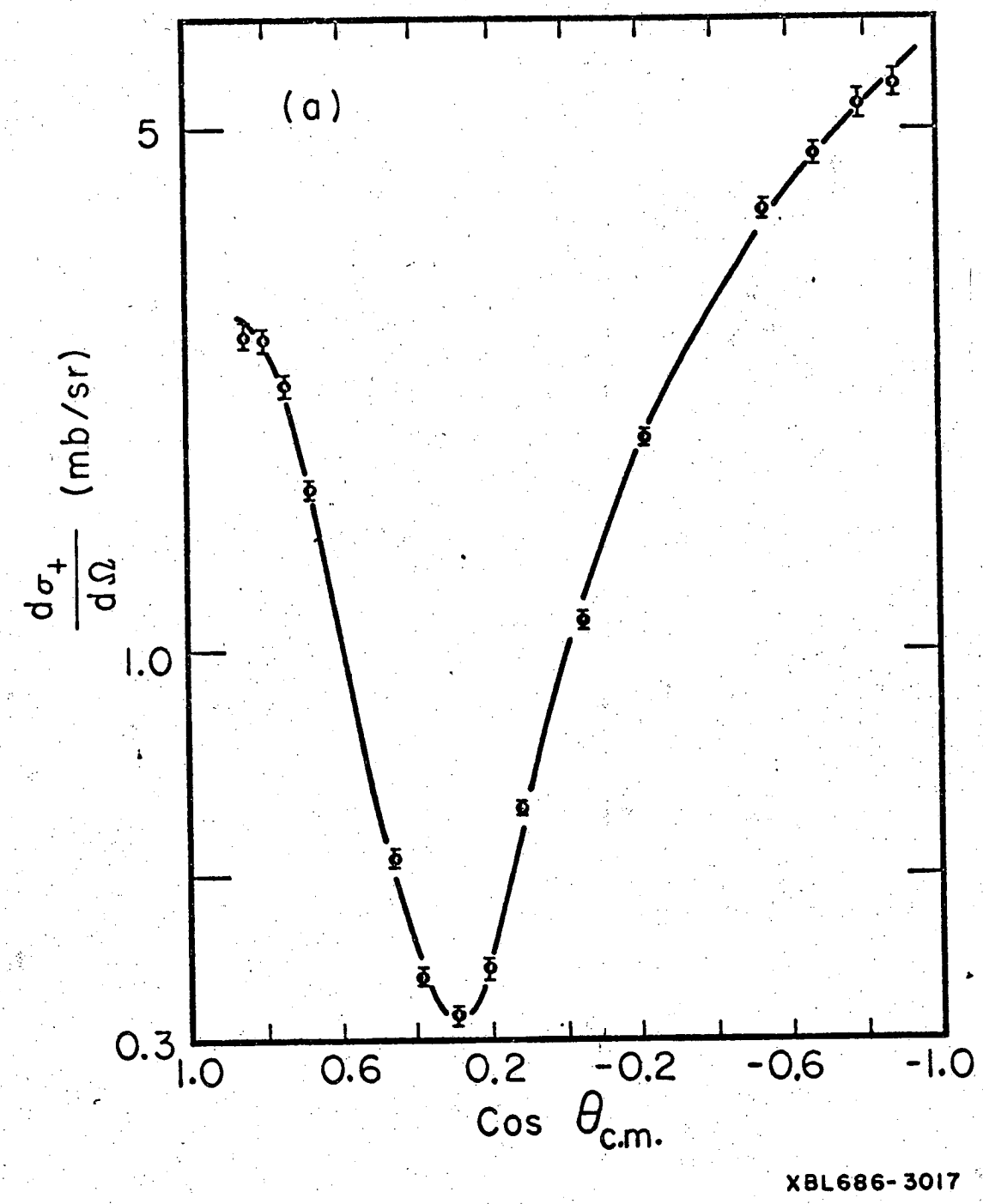
(a)
5
1.0
0.3
$\frac{d\sigma_+}{d\Omega}$ (mb/sr)
1.0
0.6
0.2
-0.2
-0.6
-1.0
Cos $\theta_{c.m.}$
XBL686-3017

Figure 8(a)

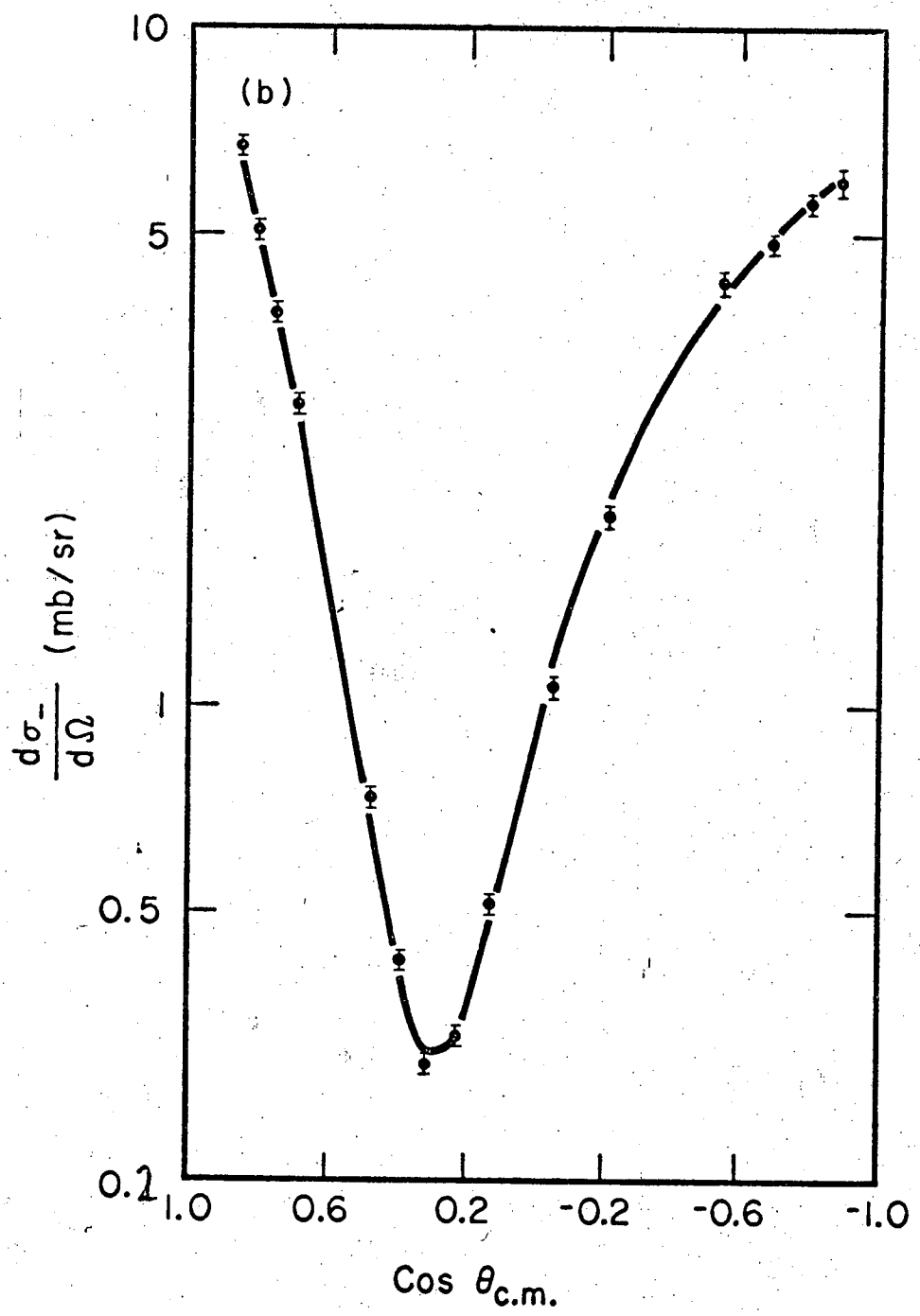
(b)
10
5
1
0.5
0.2
$\frac{d\sigma_-}{d\Omega}$ (mb/sr)
1.0
0.6
0.2
-0.2
-0.6
-1.0
Cos $\theta_{c.m.}$
XBL6810-6848

Figure 8(b)

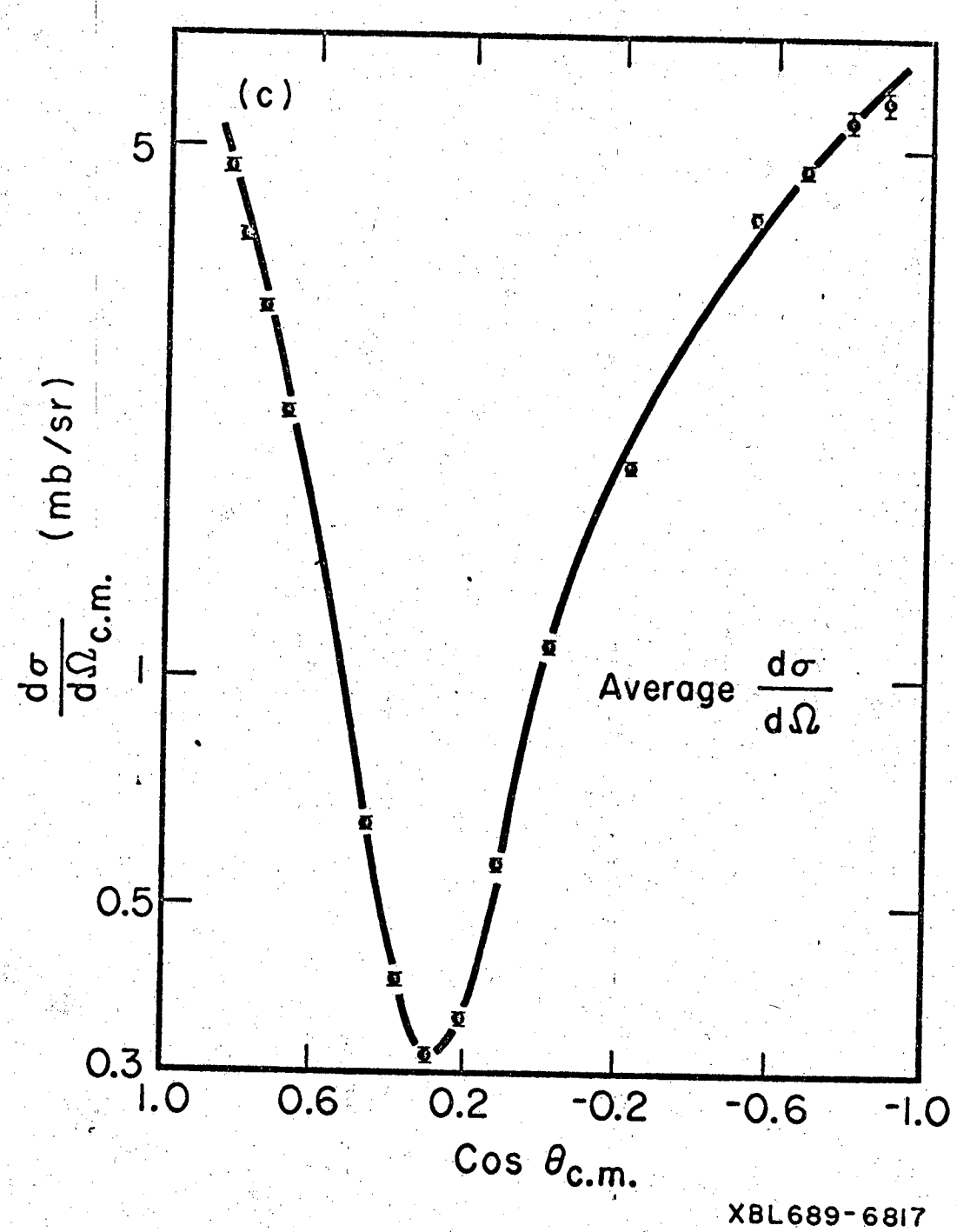
(c)
5
1
0.5
0.3
$\frac{d\sigma}{d\Omega}_{c.m.}$ (mb/sr)
Average $\frac{d\sigma}{d\Omega}$
1.0
0.6
0.2
-0.2
-0.6
-1.0
Cos $\theta_{c.m.}$
XBL689-6817

Figure 8(c)

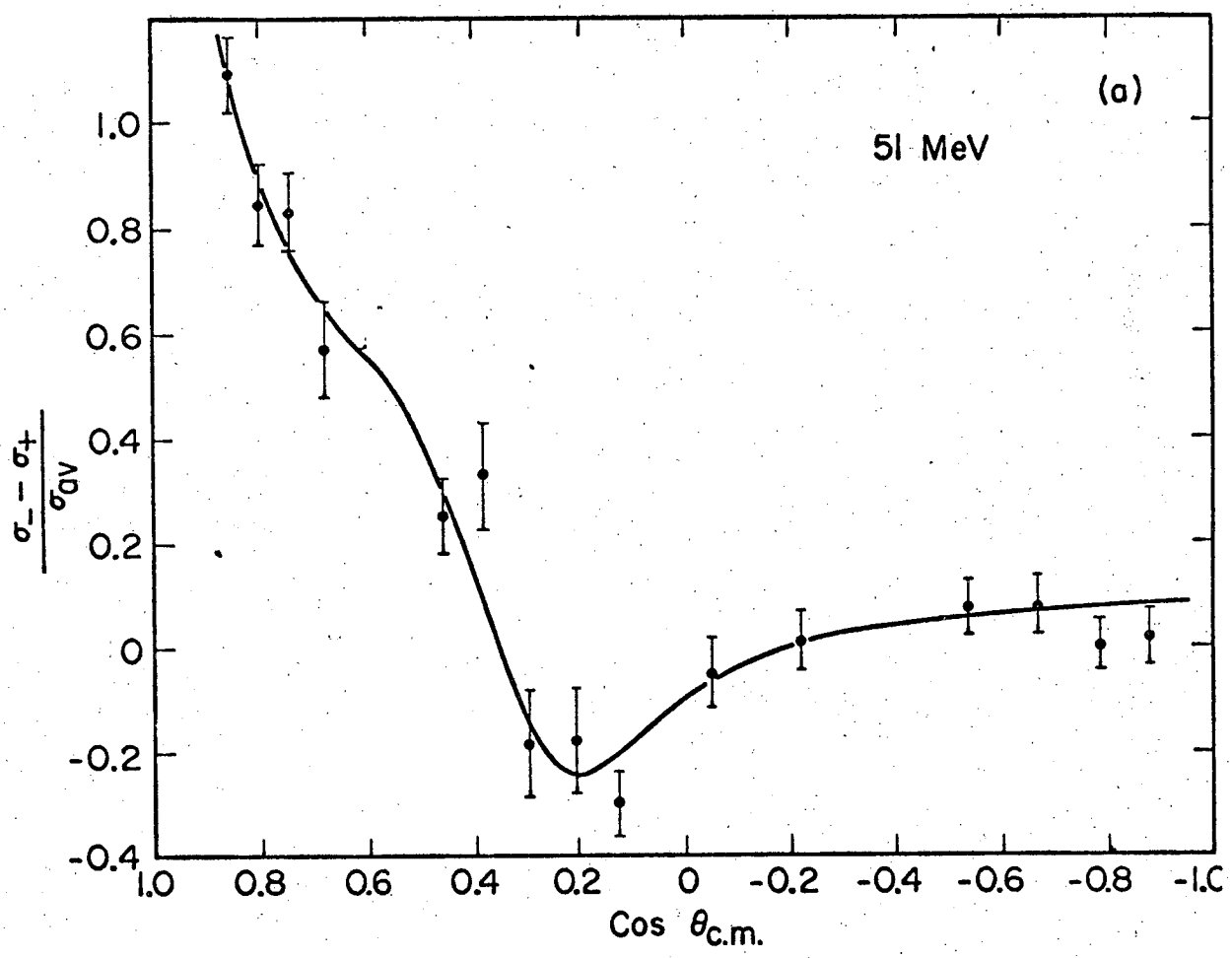

XBL686-3013

Figure 9(a)

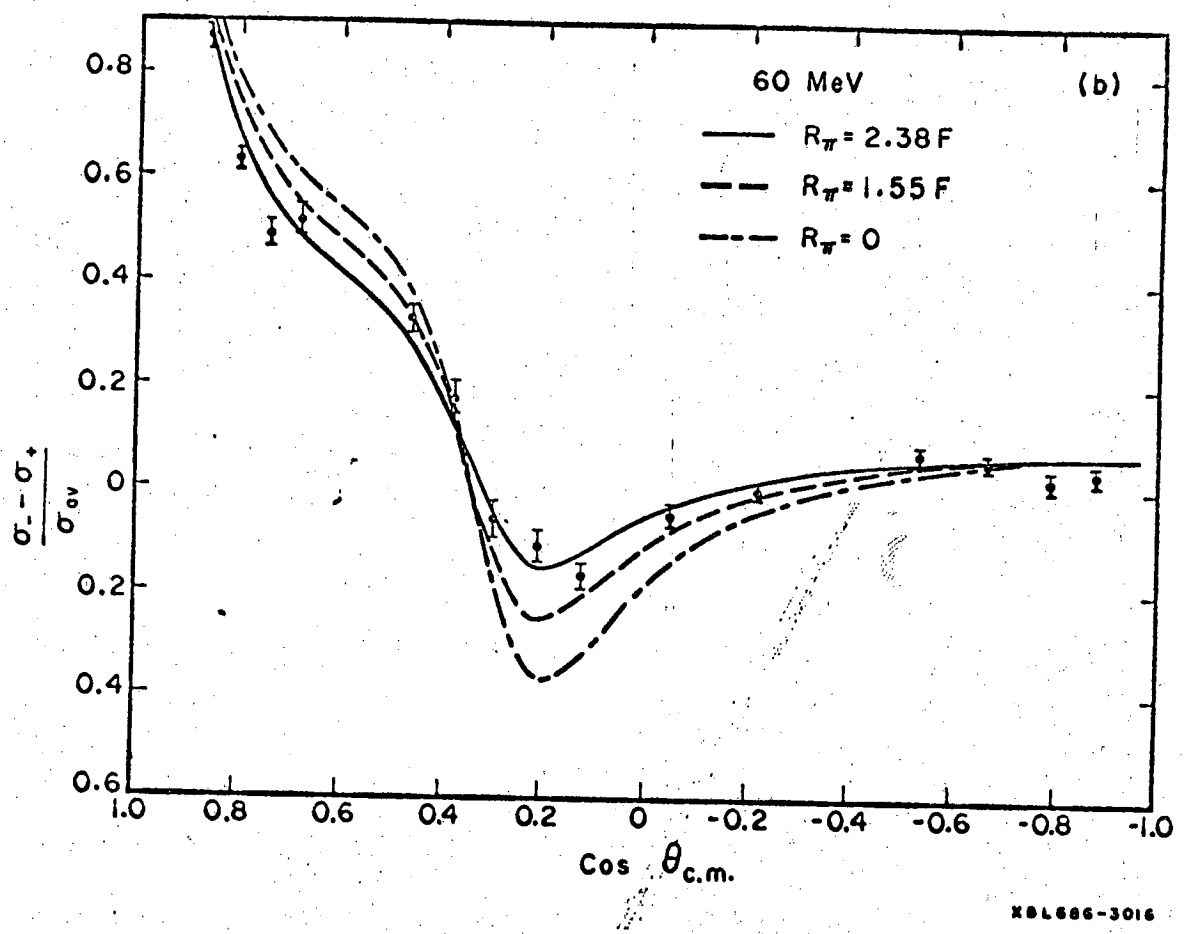
60 MeV
(b)
R_π = 2.38 F
R_π = 1.55 F
R_π = 0
$\frac{\sigma^- - \sigma^+}{\sigma^{av}}$
0.8
0.6
0.4
0.2
0
0.2
0.4
0.6
1.0
0.8
0.6
0.4
0.2
0
-0.2
-0.4
-0.6
-0.8
-1.0
Cos $\theta_{c.m.}$
XBL686-3016

Figure 9(b)

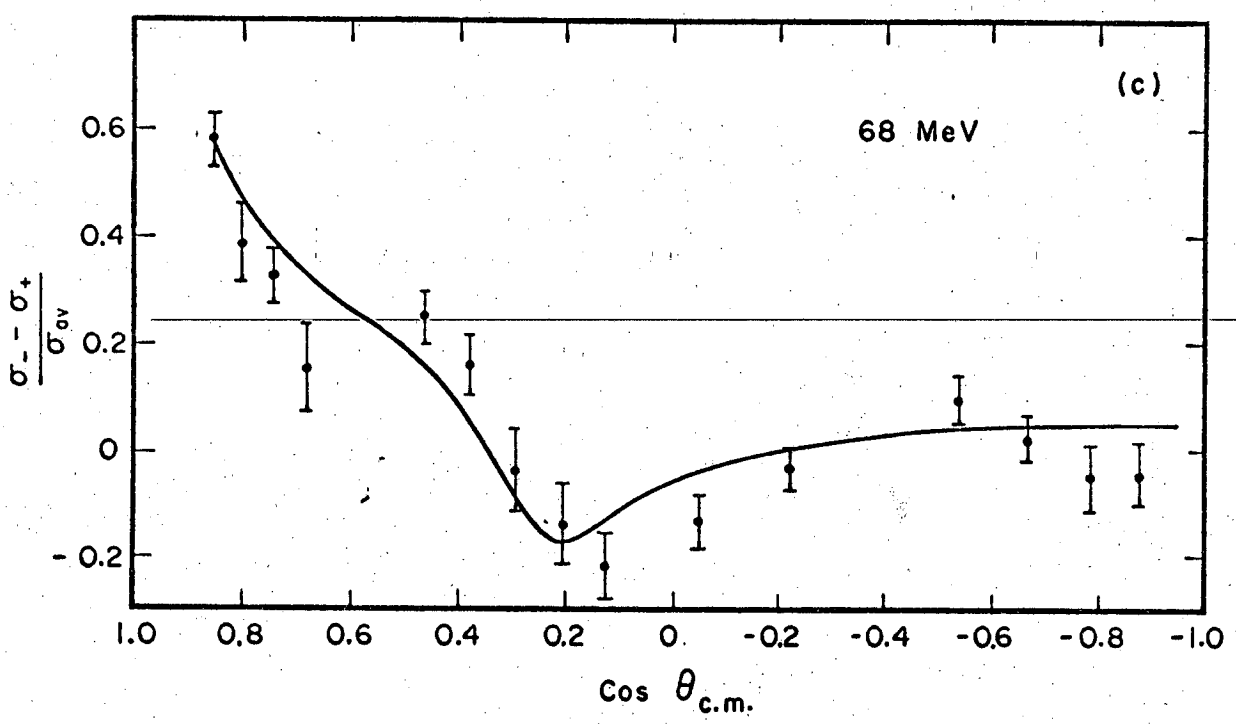
(c)
68 MeV
0.6
0.4
0.2
0
- 0.2
$\frac{\sigma_- - \sigma_+}{\sigma_{av}}$
1.0
0.8
0.6
0.4
0.2
0.
-0.2
-0.4
-0.6
-0.8
-1.0
Cos $\theta_{c.m.}$
XBL686-3015

Figure 9(c)

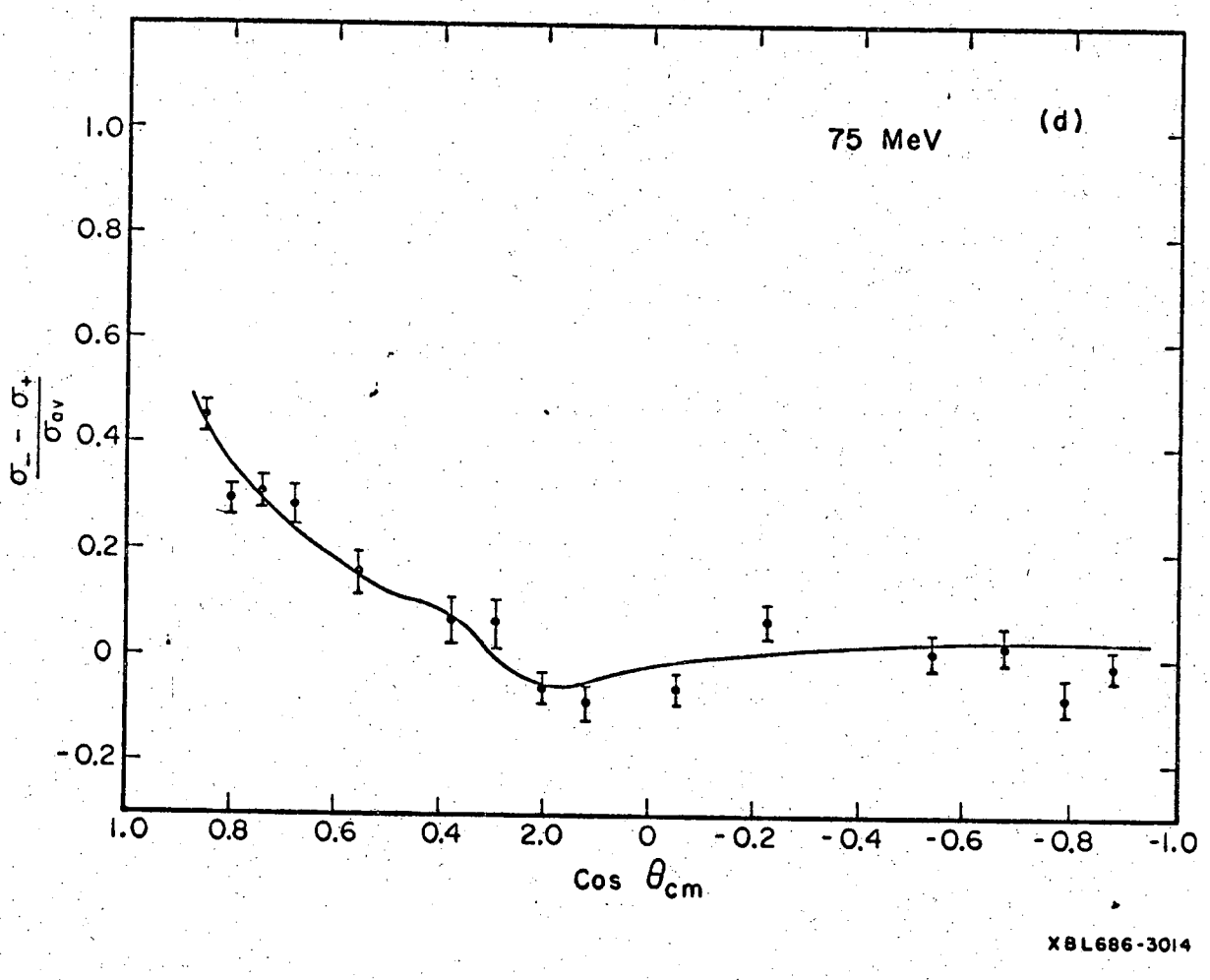
75 MeV
(d)
1.0
0.8
0.6
0.4
0.2
0
-0.2
$\frac{\sigma_- - \sigma_+}{\sigma_{av}}$
1.0
0.8
0.6
0.4
2.0
0
-0.2
-0.4
-0.6
-0.8
-1.0
Cos θ_{cm}
XBL686-3014

Figure 9 (d)

Table II. Data for each of the four energies in the form of differential cross sections as a function of $\theta_{c.m.}$

$\theta_{c.m.}$ (deg)	$\frac{d\sigma+}{d\Omega}$ (mb/sr)	ϵ_+ (mb/sr)	$\frac{d\sigma+}{d\Omega}$ (mb/sr)	ϵ_- (mb/sr)
51 MeV				
31.5	1.516	0.140	5.192	0.254
36.7	1.611	0.136	3.969	0.166
41.9	1.223	0.093	2.978	0.145
47.1	1.131	0.093	2.033	0.107
62.5	0.434	0.024	0.560	0.025
67.6	0.266	0.023	0.371	0.020
72.7	0.323	0.020	0.269	0.019
77.8	0.375	0.023	0.314	0.020
82.8	0.581	0.026	0.427	0.023
92.9	0.993	0.050	0.950	0.041
102.8	1.610	0.057	1.638	0.053
122.5	3.433	0.144	3.715	0.132
132.2	4.095	0.164	4.471	0.148
141.8	4.764	0.177	4.791	0.147
151.4	4.918	0.194	5.034	0.156
60 MeV				
31.5	2.661	0.075	6.712	0.146
36.7	2.634	0.071	5.033	0.106
41.9	2.327	0.052	3.854	0.076
47.1	1.663	0.046	2.835	0.062
62.6	0.534	0.010	0.747	0.013
67.7	0.366	0.009	0.436	0.009
72.8	0.325	0.008	0.306	0.008
77.9	0.375	0.008	0.336	0.009
83.0	0.618	0.012	0.521	0.011
93.0	1.128	0.021	1.077	0.021
102.9	1.928	0.031	1.916	0.031
122.6	3.936	0.079	4.232	0.083
132.3	4.592	0.104	4.875	0.109
141.9	5.422	0.150	5.544	0.153
151.5	5.721	0.196	5.924	0.203
68 MeV				
31.6	4.031	0.190	7.299	0.273
36.8	3.612	0.176	5.312	0.361
42.0	3.247	0.135	4.494	0.164
47.2	2.651	0.126	3.082	0.223
62.7	0.722	0.025	0.925	0.034
67.8	0.437	0.020	0.512	0.026
72.9	0.382	0.018	0.366	0.022
78.0	0.447	0.019	0.388	0.025
83.1	0.692	0.025	0.556	0.030
93.1	1.350	0.047	1.180	0.051
103.0	2.094	0.063	2.018	0.069
122.7	4.011	0.149	4.392	0.142
132.4	4.961	0.176	5.098	0.163
142.0	5.853	0.213	5.543	0.316
151.5	5.843	0.267	5.591	0.333
75 MeV				
31.6	5.940	0.205	9.394	0.236
36.9	5.252	0.167	7.080	0.215
42.1	4.268	0.141	5.858	0.132
47.3	3.006	0.104	3.979	0.127
62.8	0.960	0.025	1.119	0.023
67.9	0.623	0.019	0.667	0.017
73.0	0.458	0.017	0.488	0.014
78.1	0.529	0.019	0.498	0.015
83.2	0.776	0.023	0.710	0.018
93.2	1.413	0.042	1.325	0.035
103.1	2.203	0.057	2.361	0.050
122.8	4.508	0.143	4.578	0.103
132.4	5.264	0.152	5.379	0.116
142.0	6.054	0.175	5.646	0.169
151.6	6.114	0.200	6.046	0.203

Figure 8 shows $\frac{d\sigma-}{d\Omega}_{c.m.}$, $\frac{d\sigma+}{d\Omega}_{c.m.}$, and $\frac{d\sigma(av)}{d\Omega}_{c.m.}$

The data in the form of differential cross sections versus $\theta_{c.m.}$ are presented in Table II.

The difference in the cross-sections divided by the average (=D/A) is shown in Fig. 9.

This variable is sensitive to R_π because it is independent of those correction factors which are the same for π^- and π^+, and because the nuclear amplitude cancels to first order. In fact, if one writes the amplitude as $f = f^N + f^D + F\, f^{pt}$ where f^D is the distortion amplitude, f^N is the pure nuclear amplitude, F the combined form factor of the pion and the alpha, and f^{pt} the point Born Coulomb amplitude then

$$D/A = 4(\mathrm{Re}\, f^N f^D + F\, \mathrm{Re} f^N f^{pt})/(|f^N|^2+|f^D|^2+ |Ff^{pt}|^2)$$

Since f^N is much larger than the other two parts of the amplitude, we are sensitive to F and f^D. The sensitivity to R_π is shown for 60 MeV.

A phase-shift analysis has been made up to the D wave. Higher partial waves were found not to be significant. The phase shifts are shown in Table III. The total inelastic cross section data of Block et al.[8] are used to constrain the imaginary phase shifts.

A. The Optical Potential Method

In this method a particular potential is postulated for the strong interaction. Following the method of Auerbach et al.,[7] a Kisslinger model[23] is used for the form of the potential.

Table III. Phase shifts (degrees)

Energy (MeV)		ReS	ImS	ReP	ImP	ReD	ImD
51	π^+	- 7.5±.5	1.6±1.8	9.0±.2	2.2±1.4	1.0±.1	.2±.3
	π^-	- 9.3±.2	1.9±1.2	9.1±.2	2.4±1.3	1.0±.2	.1±.1
60	π^+	- 8.0±.5	2.9±.8	11.4±.3	1.4±1.0	1.6±.1	.3±.3
	π^-	-10.4±.3	2.0±1.2	11.4±.5	3.3±1.8	1.4±.1	.7±.4
68	π^+	- 8.6±.5	1.7± .8	13.4±.5	3.7± .7	2.1±.1	.6±.2
	π^-	-11.0±.5	2.4±1.8	12.8±.5	4.1±2.0	1.7±.2	.8±.1
75	π^+	- 7.9±1.4	.1±1.6	15.5±.5	7.2±1.8	2.8±.3	.6±.5
	π^-	-10.7± .9	1.6±2.2	15.2±.5	6.2±3.3	2.7±.2	.8±.2

A derivation of the optical model is given by Watson[24] and repeated by Auerbach et al.[7] In scattering a pion off a nucleus of A nucleons, we can write the Hamiltonian as

$$H = (H_N + h) + \sum_{i=1}^{A} V_i \equiv H_0 + V$$

where H_N is the nuclear Hamiltonian, h the pion kinetic energy operator and V the pion-nucleon potential. The scattering amplitude satisfies the Lippman-Schwinger equation

$$T\psi = \left(V + V \frac{1}{E-H_0+i\epsilon} T\right)\psi \qquad (1)$$

where E is the usual eigen value of H_0. The solution of (1) is

$$T = \sum_{i}^{A} t'_i + \sum_{iji}^{A,} t'_i \frac{1}{E-H_o+i\epsilon} t'_j + \sum_{ijk}^{A,} t'_i \frac{1}{E-H_o+i\epsilon} t'_j \frac{1}{E-H_o+i\epsilon} t'_k + \ldots$$

where t'_i is the bound pion-nucleon scattering amplitude and Σ' excludes successive scatters by the same nucleon.

The elastic scattering amplitude is

$$T_E = \Sigma t'_{iE} + \Sigma (t'_i \frac{1}{E-H_0+i\epsilon} t'_j)_E + \ldots\ldots \qquad (2)$$

where the E subscript denotes a scatter with the nuclear energy unchanged. T_E then, is the elastic scattering amplitude. Now, in analogy with (1), we write

$$T_E = V_o + V_o \frac{1}{E-H_o + i\varepsilon} T_E \qquad (3)$$

where V_o is the optical potential. Now the problem is change from a multi-body problem to one with one particle of Hamiltonian H_o. A few approximations are made. First, excited nuclear states are ignored. This allows us to set

$$\left(t'_i \frac{1}{E-H_o + i\varepsilon} t'_j \frac{1}{E-H_o + i\varepsilon} \right)_E = t'_{iE} \frac{1}{E-H_o + i\varepsilon} t'_{jE} \frac{1}{E-H_o + i\varepsilon}$$

(for the alpha, the first excited state is about 20 MeV away--we have already neglected them all in assuming I=0). Now we assume $\Sigma=\Sigma'$, which is valid if A is large or if the two body forces are weak. Then, equations (2) and (3) imply that $V_o = \Sigma t'_{iE}$
Now, the impulse approximation is used, which involves replacing the bound amplitudes by free ones. This is permissible for energies substantially larger than the nuclear binding energies. Then, neglecting nuclear recoil, we can write in momentum space

$$\langle \vec{p}' | V_o | \vec{p} \rangle = \Sigma \langle \vec{p}' | t_i | \vec{p}) \rho(\vec{p}-\vec{p})$$

where $\vec{p}$ and $\vec{p}'$ are the pion momenta and $\rho(\vec{p}-\vec{p})$ is the Fourier transform of the nuclear density normalized to unity.

The simplest model assumes

$$\langle \vec{p}' | t | \vec{p} \rangle \simeq \langle \vec{p} | t | \vec{p} \rangle \rho(\vec{p}-\vec{p}) \qquad (4)$$

which means that $\rho\ (\vec{p}-\vec{p}')$ is peaked about the incident momentum. Inverting this into co-ordinate space, we get

$$V_o(r) = (2\pi)^3\ A\langle\vec{p}|t|\vec{p}\rangle\rho_N(\vec{r})$$

where $\langle\vec{p}|t|\vec{p}\rangle$ is the average over π-n and π-p scattering, and $\rho_N(\vec{r})$ is the nuclear density. This assumption is known as the local potential model, containing only an S-wave term. This neglects the fact that low energy pion-nucleon scattering has a strong P-wave dependence, notably the diffraction dip somewhat below 90 deg., and this model has not been successful in fitting data.

Kisslinger's improvement on the local potential was, in fact, to introduce a P-wave part explicitly into the matrix element for the scattering amplitude $\langle\vec{p}|t|\vec{p}\rangle = a_o + a_1 p^2 \cos\theta = a_o + b_1\ \vec{p}\cdot\vec{p}'$ The p^2 term is used since usually $t_\ell \sim p^{2\ell}$ for low energy scattering. The co-ordinate space representation is then

$$V_o(\vec{r}) = (2\pi)^3 A(a_o\rho_N(\vec{r}) + a_1\vec{p}\cdot\rho_N(r)\vec{p})$$

or, in operator notation,

$$V_o(\vec{r})\psi = (2\pi)^3\ A(a_0\rho_N(\vec{r})\ \psi + a_1\ \vec{\nabla}\cdot\ (\rho_N(\vec{\nabla})\cdot\ \vec{\nabla}\psi))$$

The Kisslinger model is experimentally valid only well below the 3-3 resonance since it takes no account of resonant behavior at 190 MeV. Clearly, this model also violates unitarity for large energies. On the other hand, we also use the impulse approximation in this discussion which requires energies much larger than 20 MeV. In our region of

60 MeV, we hope to satisfy both requirements.

The modified Klein-Gordon equation is used with $U = 2E_\pi V_o$ inserted at the scalar component of a four-vector

$$(-\nabla^2 + \mu^2)\psi = [(E_\pi - V_c)^2 - U]\psi$$

with E_π the energy of the pion, V_c the Coulomb potential, μ the pion mass. Terms of order $V_c V_o$ and V_o are dropped.
The following variables are defined:

$$b_0 = -2(2\pi)^3 E_\pi a_0/p^2$$
$$b_1 = -2(2\pi)^3 E_\pi a_1$$

so that

$$U\psi = [-Ab_0 p^2 \rho_N(\vec{r}) + Ab_1 \vec{\nabla}\cdot\{\rho_N(\vec{r})\vec{\nabla}\}]\psi$$

Now, b_0 and b_1 are the complex optical parameters which are introduced to represent the S- and P- wave πN scattering, respectively.

The optical parameters can be theoretically related to the πN phase shifts as follows:

$$\text{Since } \langle\vec{p}|t|\vec{p}\rangle_{Lab} = -f(0)_{lab}/(4\pi^2 E_\pi)$$

and $f(0)_{lab}/p_{lab} = f(0)_{cm}/k_{cm}$ from the optical theorem and the invariance of total cross sections, for $\ell = 0,1$

$$b_\ell = \frac{4\pi}{p_{lab}^3} \quad \frac{\mu^2 + M_N + 2E_\pi M_N}{M_N^2} \quad [kf(0)_{cm}]_\ell$$

and if $\alpha_i = \frac{e^{2i\delta_{i-1}}}{2}$ with δ_i the phase shifts and i = (2T, 2J) for isospin and spin indices, we have for π^- and an (A, Z) nucleus where Z is the number of protons.

$$[kf(0)_{cm}]_0 - \frac{1}{A}\left[\frac{Z}{3}\alpha_3 + 2\alpha_1 + (A-Z)\alpha_3\right]$$

$$[kf(0)_{cm}]_1 = \frac{1}{A}[Z(2\alpha_{33} + \alpha_{31} + 4\alpha_{13} + 2\alpha_{11})\ 3 + (A-Z)\ (2\alpha_{33} + \alpha_{31})]$$

For π^+, Z and A-Z are interchanged.

In rewriting the equation to allow for the recoil of the α particle and provide for relativistic kinematics, a modification[25] of the expression of Goldberger and Watson[26] is used:

$$(\nabla^2 + k^2)\psi = (2E_{eq}\ V_c + (1 - 3E_{eq}/W)\ V_c^2 - U)\psi.$$

where E_{eq} is the equivalent relativisitic one-particle c.m. energy, W is the total c.m. energy, and k is the c.m. momentum.[27]

This center-of-mass equation is solved for the radial wave functions. Given b_0, b_1, E_{eq}, $\rho_N(r)$, and V_c, cross sections are obtained for the solutions by matching logarithmic derivatives at 4F., well outside the nuclear surface, to the external Coulomb wave functions in the conventional way. For a given energy, then, there are six parameters which lead to predicted cross sections: the real and imaginary parts of b_0 and b_1, and radius parameters for $\rho_N(\vec{r})$ and for $\rho_c(\vec{r})$. A Gaussian form is taken both for the nuclear density $\rho_N(\vec{r})$ and the combined π-He

Table IV. Optical parameters, and radial parameters obtained by optical-model fits at each energy.

T_π (MeV)	$Reb_0(F^3)$	$Imb_0(F^3)$	$Reb_1(F^3)$	$Imb_1(F^3)$	a(F)	$R_c(F)$	$R_\pi(F)$	χ^2 (D/A)	χ^2 (av)	χ^2	χ^2 exptd.	Phase-shift method R_π	χ^2 exptd.	χ^2
51.3	-2.94±.10	.099±.28	5.83±.30	.100±.40	1.25±.04	2.37±.30	2.39±.45	16.7	23.8	40.5	24		16	34.9
59.7	-2.63±.09	-.165±.17	5.96±.20	.167±.25	1.26±.04	2.37±.18	2.39±.27	39.2	53.9	93.1	24		16	85.8
67.6	-2.26±.11	-.568±.19	6.10±.30	.797±.39	1.19±.04	2.13±.33	2.02±.52	27.2	25.1	52.3	24	2.96±.43	16	39.1
75.0	-2.18±.11	-.480±.18	6.22±.24	.567±.35	1.20±.04	2.38±.28	2.40±.42	28.6	29.5	58.1	24		16	52.1

Table V. Error matrix for best fit at 60 MeV.

	Reb_0	Imb_0	Reb_1	Imb_1	a_N	R_c
Reb_0	1.5×10^{-4}	-1.4×10^{-4}	-4.4×10^{-4}	1.6×10^{-4}	1.4×10^{-4}	3.4×10^{-4}
Imb_0		5.8×10^{-4}	-7.8×10^{-4}	-1.6×10^{-3}	-9.9×10^{-5}	-8.7×10^{-4}
Reb_1			5.5×10^{-3}	4.3×10^{-3}	-6.6×10^{-4}	3.6×10^{-4}
Imb_1				6.3×10^{-3}	-8.7×10^{-5}	2.4×10^{-3}
a_N					1.6×10^{-4}	3×10^{-4}
R_c						5.8×10^{-3}

charge density $\rho_c(\vec{r})$:

$$\rho_N(r) = A \exp(-r^2/a^2)/[(\pi)^{1/2}a]^3 \text{ and } \rho_c(r) = Ze \exp(-r^2/R_c^2)[\pi^{1/2}R_c]^3.$$

The Coulomb radius parameter is related to the rms radius of the pion by $R_\pi^2 = 1.5\ R_c^2 - R_{He}^2$, with $R_{He} = 1.65 \pm .03$ F, from electron scattering experiments.[28,29]

An optimum set of parameters is found by searching for the best fit to the data. A fit is made simultaneously to the average cross section and to the D/A data.

The parameters b_0, b_1, a, and R_c obtained by this direct method of fitting the data with an optical model are listed in Table IV. The errors quoted are derived from the diagonal elements of the error matrix shown in Table V. R_c's diagonal element is sufficiently larger than its off-diagonal elements, so that the error quoted for R_c, and consequently for R_π, is, we believe, reliable. The errors on the parameters in the table also include uncertainties in absolute and relative $\pi^- - \pi^+$ normalization.

The values of χ^2 obtained by using statistical errors only for the best fits are somewhat larger than expected from the numbers of degrees of freedom. In propagating the errors of the data to include systematic errors, we have increased the estimate of the errors by an appropriate factor $(\chi^2/\chi^2_{\text{expected}})^{1/2}$. The fits to the D/A data are better than those for the average, since some systematic errors in the experimental corrections made for a particular angle would cancel in D/A.

In Figs. (10 & 11) we show the values for the optical parameters predicted from phase shifts for A=2Z, and some results for other elements [7]. We also show the values obtained from our data. Re b_1 agrees well. Re b_0 differs sharply from the prediction, but our data agrees with other experimental results. Auerbach surmises[7] that this divergence is due to the deviations from free πN amplitudes. In theory, Re $b_0^N(2\delta_3 + \delta_1)/p^3$ which is fairly constant due to accidental cancellations of the terms linear in p. These accidental cancellations can then be easily spoiled if the impulse approximation is only slightly wrong, resulting in a $1/p^2$ dependence, which is what is found.

Our data for Im b_1 falls below predicitions (as does other data) and our values for Im b_0 have the wrong sign for three of our four energies and this parameter is not plotted. A possible reason for these discrepancies is explained below. The Lorentz-Lorenz effect has been neglected here. The inclusion of the Lorentz-Lorenz effect involves replacing $Ab_1\rho_N(r)$ by $Ab_1\rho_N(r)/[1 - \frac{1}{3}Ab_1\rho_N(r)]$ in analogy to the scattering of an electromagnetic wave by a polarizable medium. (See M. Ericson and T. E. O. Ericson, Ann. Phys. 36, 326-362 (1966).) When this is done in the search routine, the optical parameters change slightly, but R_c varies only by about 3%.

It should be emphasized that the relation of πN amplitudes to optical parameters is heavily dependent on the assumptions mentioned above. The impulse approximation has been used, excited nuclear states have been neglected, and two-body forces have been assumed to be weak. Also, nuclear recoil has been neglected, which may be in error, especially

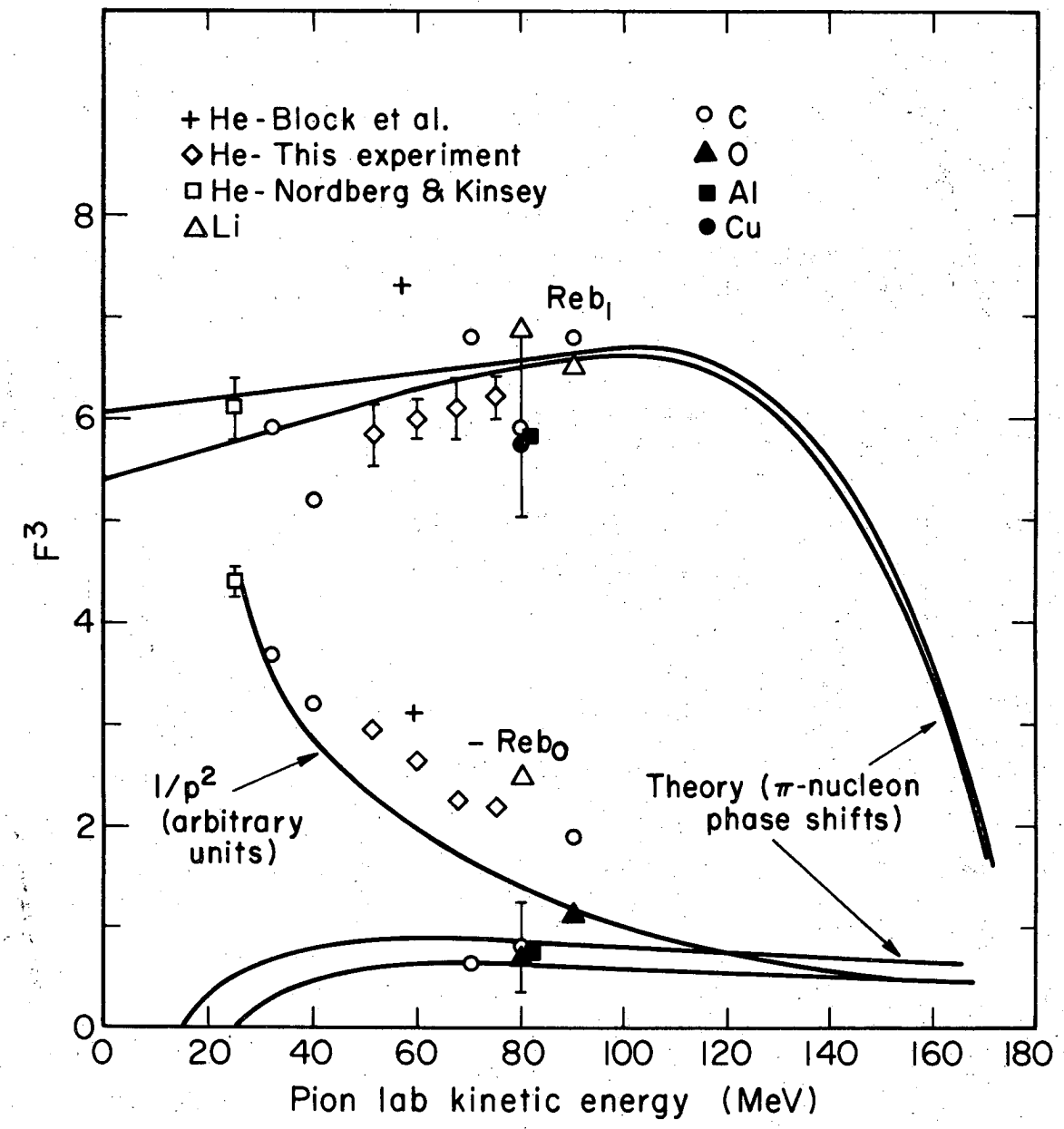

XBL695-2758

Fig. 10

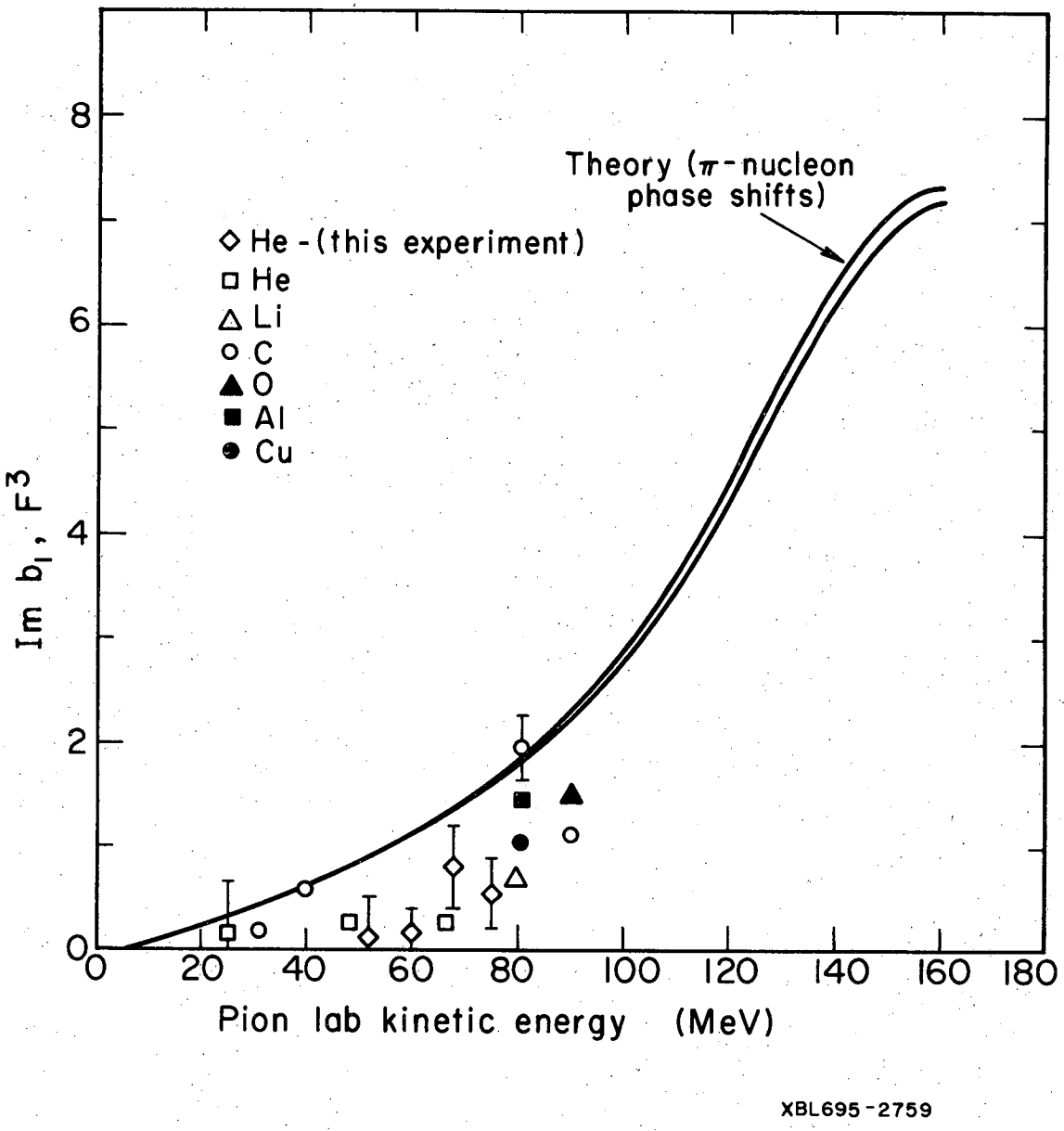
Theory (π - nucleon phase shifts)
◇ He - (this experiment)
□ He
△ Li
○ C
▲ O
■ Al
● Cu
Im b_1, F^3
0
2
4
6
8
0
20
40
60
80
100
120
140
160
180
Pion lab kinetic energy (MeV)
XBL695-2759

Fig. 11

for off-mass-shell terms in the matrix elements of V_o which contribute to large angle scattering.[30,31] The Kisslinger model has, however,[32] been successful in fitting pion-nuclear scattering at low energies, whereas the local potential model has failed.

A problem in this analysis has been pointed out by Baker et al.[32] The radial wave equation arising from (1) is

$$\frac{d^2\chi_\ell}{dr^2} + p(r)\frac{d\chi_\ell}{dr} + q(r)\,\chi_\ell = 0,$$

$$\text{where } p(r) = \frac{2}{r} + \frac{\frac{d\rho_N(r)}{dr}}{1 + Ab_1\rho_N(r)}$$

$$\text{and } q(r) = \frac{k^2 - Ab_0\rho_N(r) - 2E_{eq}V_c - (1-3E_{eq}/W)V_c^2}{1 + Ab_1\rho_N(r)} - \frac{\ell(\ell+1)}{r^2}$$

Because of the term $1 + Ab_1\rho_N(r)$ in the denominators of the coefficients, there is a regular singular point in the equation when $Ab_1\rho_N(r) = -1$.[33]

Since A and $\rho_N(r)$ are real, the denominator factor, $1 + Ab_1\rho_N(r)$, induces a logarithmic branch point in the radial wave function, for $Reb_1 = -1/A\rho_N(r)$ and $Imb_1 = 0$. For Imb_1 small, the singularity becomes a sharp peak. The presence of the singularity means that certain regions of the optical parameter space are forbidden implicitly by the model.[34] Because of the coupling between Imb_0 to a slightly positive

value, which violates unitarity.[35]

Further, this close approach to a singularity gives a peak in the radial wave function at Re $b_1 = -1/A\ \rho_N(r)$ when Imb_1 is small, as it is for the best fits. The peak has no apparent physical significance and may be considered a failure of the theory.

B The Phase-Shift Method

Another method of anlaysis uses the optical model only to calculate the distortion amplitudes in the hope of reducing the model dependence. However, there is still a dependency which cannot be removed (see part C of the analysis.) The phase-shift analysis is used to obtain amplitudes for π^+ and π^- scattering.

If one writes the total amplitude as the sum of a nuclear amplitude, f^N, a distortion amplitude, f^D, and the point Coulomb amplitude, f^{pt}, the total cross section is

$$\frac{d\sigma\pm}{d\Omega} = |f^N \pm f^D \pm Ff^{pt}|^2.$$

This equation is solved to find the form factor, F, for each data point at each energy, giving

$$F = A + B,$$

where
$$A = \left(\frac{d\sigma+}{d\Omega}_{c.m.} - \frac{d\sigma}{d\Omega}_{c.m.}\right)/4\ \mathrm{Re}\ f^N\ f^{pt}$$

and
$$B = -4\ \mathrm{Re}\ f^N\ f^D/4\ \mathrm{Re}f^N\ f^{pt}.$$

The measured quantity is A and the distortion effect is B. Where

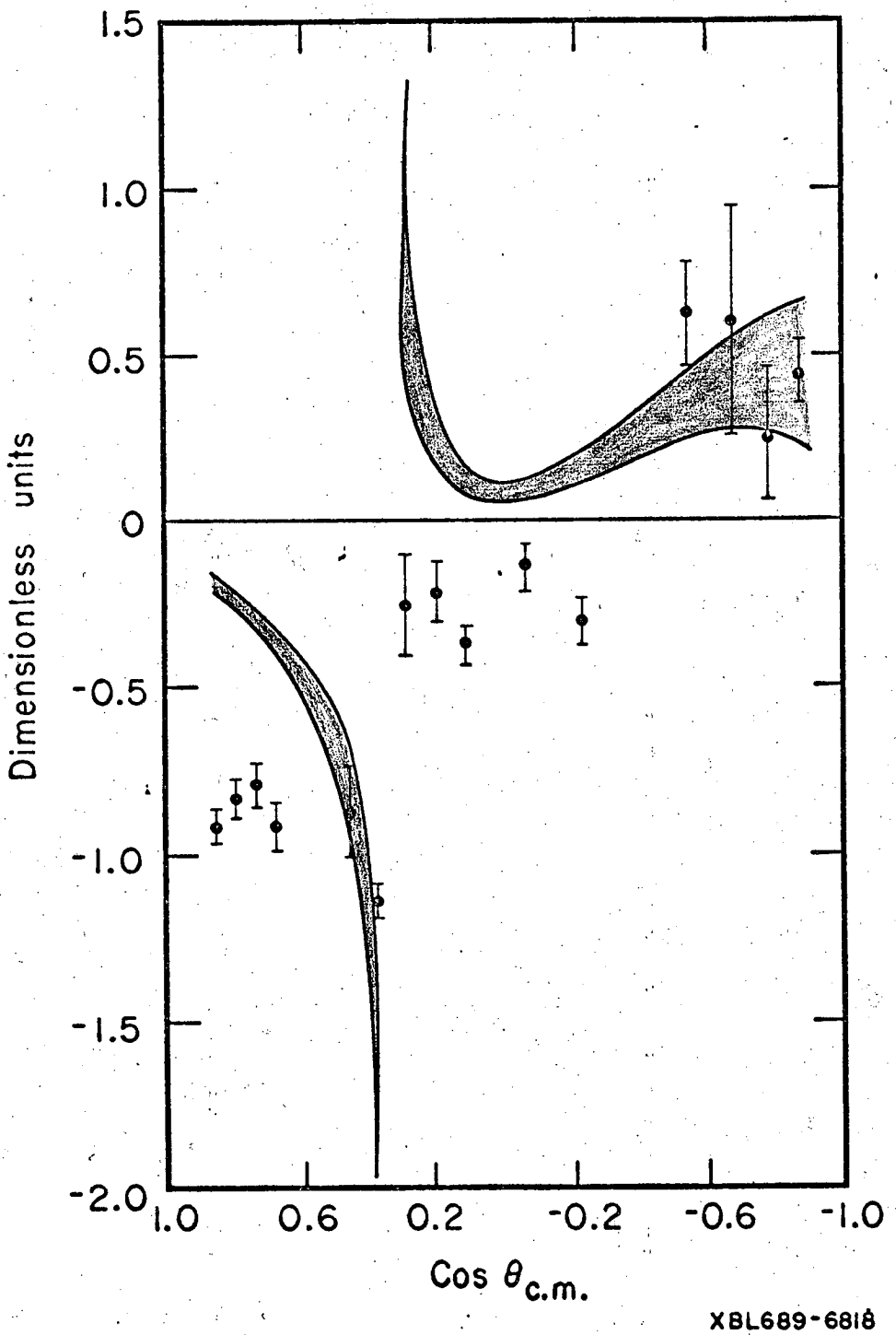
1.5
1.0
0.5
0
-0.5
-1.0
-1.5
-2.0
Dimensionless units
1.0
0.6
0.2
-0.2
-0.6
-1.0
Cos θc.m.
XBL689-6818

Figure 12

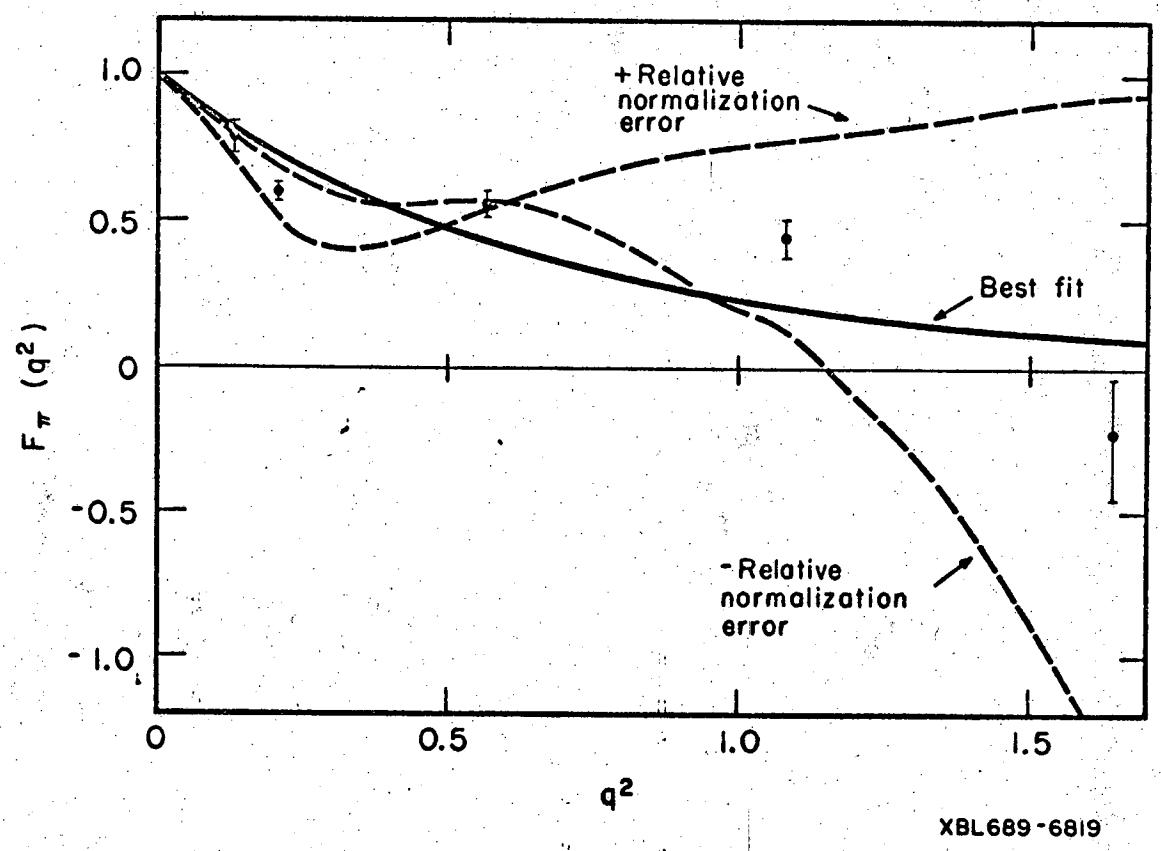
1.0
0.5
0
-0.5
-1.0
0
0.5
1.0
1.5
F_π (q^2)
q^2
+Relative normalization error
Best fit
-Relative normalization error
XBL689-6819

Figure 13(a)

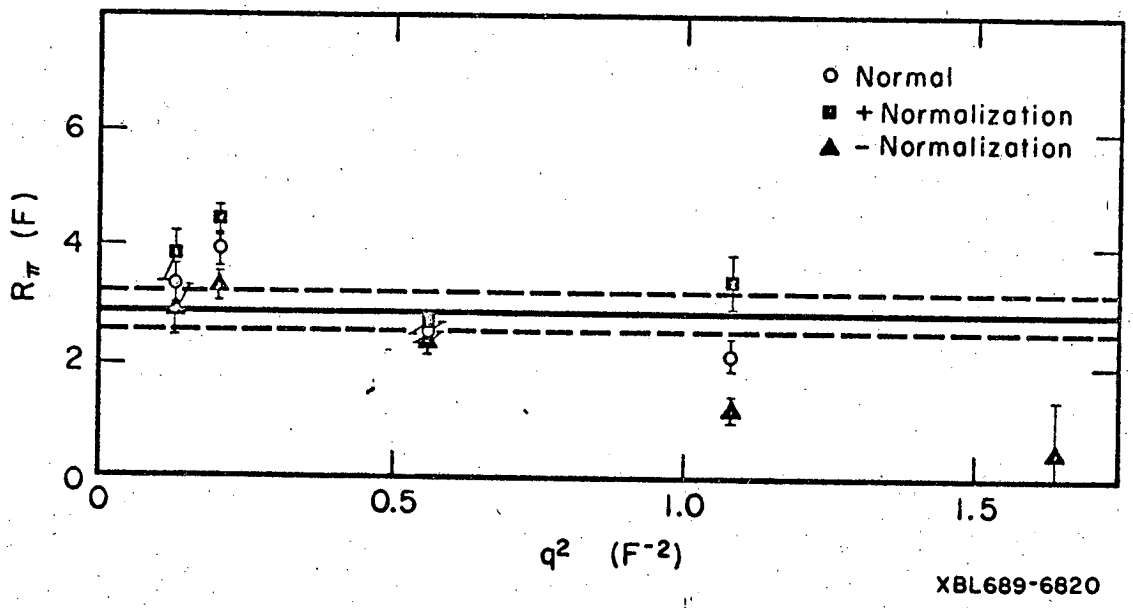
Normal
+ Normalization
- Normalization
R_π (F)
0
2
4
6
0
0.5
1.0
1.5
q^2 (F^{-2})
XBL689-6820

Figure 13(b)

A>>B, the distortion effect is negligible.

The distortion amplitude is calculated following Auerbach [7] (See Appendix). In Fig. 12, -A and B vs cos $\theta_{c.m.}$ for 60 MeV are shown. This figure shows that f^D is extremely important in determining F. Combining all the data for the various energies, we can plot F_π (q^2) vs q^2 (Fig. 13a). Assuming a Gaussian charge distribution for the helium and pion $F = \exp(-q^2 R^2/6)$ with $R_\pi^2 + R_{He}^2$, we fit the $F_\pi(q^2)$ to Find R_π. The result is 2.96 ± 0.43F. In assigning the error the same χ^2 factor mentioned in part A is used.

This error does not include the uncertainty in the form factor due to the error in the relative normalization of the π+ and π- data. This is displayed in Fig. (13a). Figure (13b) shows the radius computed independently for each F_π (q^2) data point with different relative normalizations. It is noted that below 1 F^{-2} the radius shows only slight sensitivity to the relative normalization. In fact, for all data points the best fit to $F_\pi(q^2)$ is almost independent of the relative normalization. At q^2>1 F^{-2} the larger fluctuations are a consequence of the insensitivity of D/A to R_π in this region (see Fig. 9). The normalization error in Table 1 common to both signs of beam has a negligible effect on the form factor.

This method can, in principle, be used to show the consistency of the form-factor measurement at different energies. In this measurement the statistics are not sufficiently accurate for this check to be made.

C. Distortion Amplitudes by Other Methods

It is interesting to compare our distortion amplitudes with those

arrived at by using other approximate calculations of f^D. West[6] obtains

$$f_\ell^D = -\int V_c(r)\ [e^{2i\delta_\ell} R_\ell^2(r) - j_\ell^2(kr) - (e^{2i\delta_\ell} - 1)/2k^2r^2]\ r^2 dr,$$

where $V_c(r) = \frac{4nk}{\pi} \int_0^\infty F_\pi(q^2)\ F_\alpha(q^2)\ j_0(qr)dq$, with a Yukawa form for F_π and a square-well density leading to $F_\alpha = 3\ j_1(qb)/qb$. Here, b is the radius of the square well. The nuclear radial wave function is R_ℓ and the nuclear phase shift is δ_ℓ. To evaluate R_ℓ West has chosen a square well; the Kisslinger model is modfied by substituting $[1-Ab_1\ \rho_N(r)]$ for $[1+ Ab_1\ \rho_N(r)]^{-1}$, following Baker et al.[33] For our case, however, the term $Ab_1\rho_N(r)$ as already mentioned passes through -1, thereby making the approximation invalid.

Block obtains for the distortion amplitude another approximation,

$$f_\ell^D = [nx_\ell\ e^{2i\delta_\ell} + (e^{2i\delta_\ell} - 1)(\eta_\ell - \eta_0)]/k,$$

correct to first order in n, where $nx_\ell = -k\int V_c(r)\ [R_\ell^2(r) - j_\ell^2(kr)]\ r^2 dr$ and η_ℓ are the Coulomb parameters defined by $\eta_\ell = \arg\Gamma(\ell + 1 + in)$ and $n = ZZ'e^2/\hbar v$ relative. Here, $V_c(r) = \frac{2nk}{r}$ erf (r/R_c). Further discussions of these two methods were given by Auvil[36] and Thurnauer.[37] Block's R_ℓ is found by using a local potential for each partial wave and a Gaussian distribution for both the nuclear and Coulomb interactions. The results for 60 MeV obtained from these equations are also presented in Table VI for comparison; the distortion amplitudes obtained by Block et al.[8] from the bubble chamber data are shown. The χ^2 cited in

Table VI. Distortion amplitudes. See text for more detailed assumptions for each method.

	Re	Im	$R_\pi^2(F^2)$	$R_\pi(F)$	χ^2	$\chi^2_{expected}$
	Method of Auerbach et al., Kisslinger model, 60-MeV data					
S	-0.0024 ± .0007	-0.010 ± .0011				
P	-0.0063 ± .0010	-0.008 ± .0009	8.29	2.88 ± 0.37	18.4	4
D	-0.0021 ± .0008	-0.003 ± .0009				
	Method of West, 60-MeV data					
S	0.00739	-0.00754				
P	-0.01114	0.00097	-0.27	<1.20 (1 s.d.)	84.0	4
D	-0.00243	-0.00010		<1.77 (2 s.d.)		
	Block integral Kisslinger model, 60-MeV data					
S	-0.00177	-0.00081				
P	-0.00566	-0.00138	5.11	2.26 ± 0.16	6.6	4
D	-0.00180	0.00113				
	Block integral and local potentials, 60-MeV data					
S	0.00215	-0.00015				
P	-0.01167	-0.00100	1.66	1.29 ± 0.82	76.1	4
D	-0.00271	0.00203				
	Block integral and local potentials, Block's 58-MeV data					
S	0.0033	-0.014				
P	-0.0141	0.0038	-0.4	< 0.9 (1 s.d.), < 2.1 (2 s.d.)		
D	-0.0019	0.0025				

Table VI are from the fits to $F_\pi(q^2)$.

Ericson has shown[38] that all the information on the pion charge radius is in the S-wave, due primarily to the S-wave overlap of the pion with the nucleus. Since the imaginary part of f^{pt} is negligible, $R_{Ref^D_{\ell=0}}$ is the important distortion amplitude to determine. It will be noted that $Ref^D_{\ell=0}$ differs in sign from method to method. The corresponding radii computed by the phase-shift method (except for Block's data, where his given radius for all his energies is quoted) are shown for each set of distortion amplitudes.

To arrive at these distortion amplitudes, an iteration process was used to calculate R_ℓ. A fit was first performed using average and D/A data. The R_π obtained by calculating the R_ℓ's then was inserted into the fitting routine. From this point, only the average data were used to fit, and the process was repeated until a value for R_π was converged upon. For the West method, the iteration stopped when R_π^2 became negative.

D. Discussion

There are some deficiencies in the optical-potential description as applied to this problem.

Firstly, although it may provide a good phenomenological fit to pion-nucleus scattering data in the sense that it attempts to include the strong p-wave π-nucleon scattering, the model itself may not be sufficient to calculate the distortion amplitudes to the accuracy required in this measurement. Secondly, as emphasized in the introduction, the optical potential is a non relativistic description of the π-He interaction. Specifically, diagrams of the type shown in Fig. 14 are

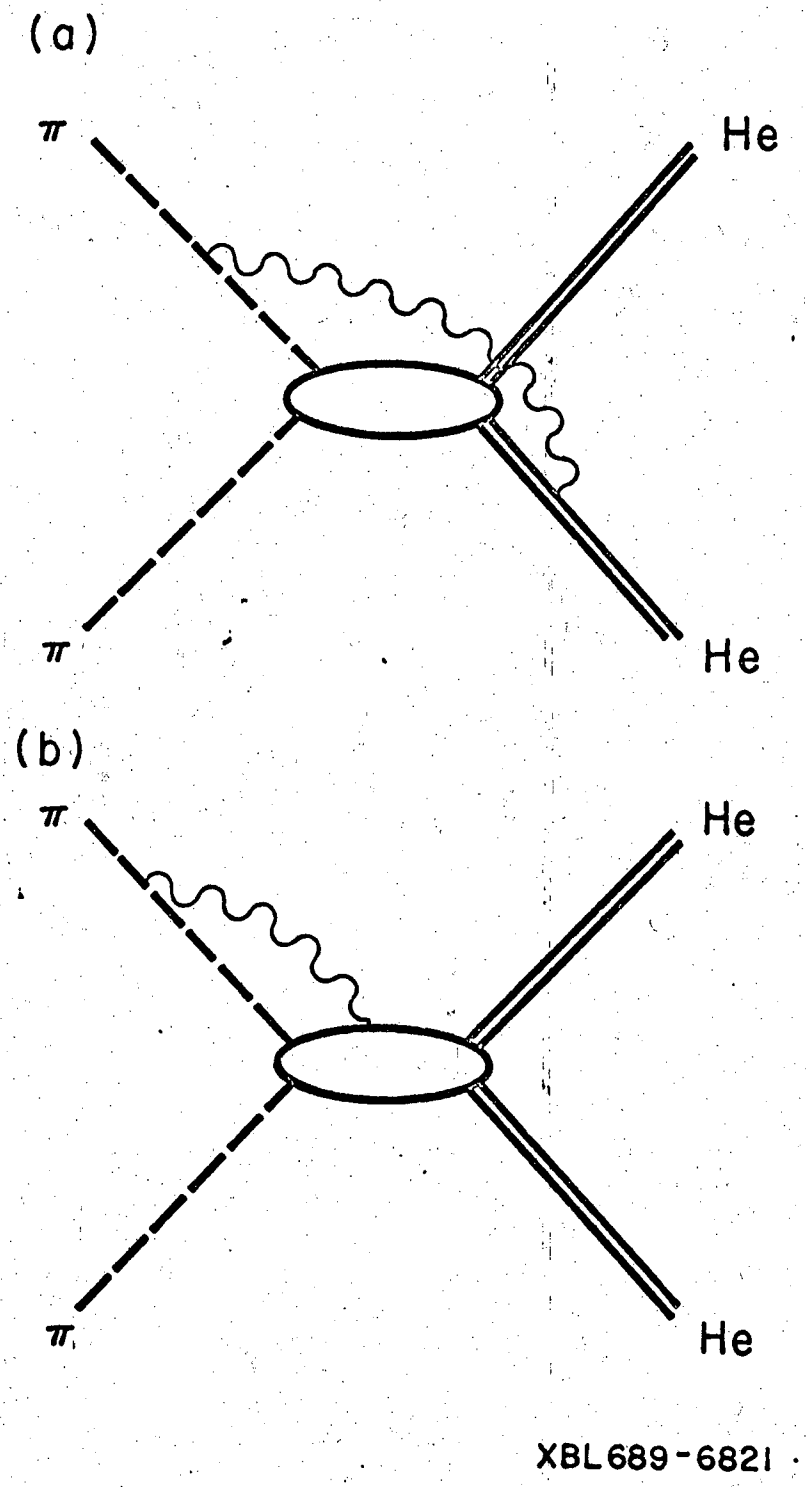

XBL689-6821

Figure 14

neglected;[10,39] such diagrams are clearly of importance for our purposes, since their amplitudes are linear in the pion charge, and a fundamental assumption in our analysis is that the only terms of this type are the pure Coulomb and the Coulomb-nuclear-distortion terms. In fact, these inner-bremsstrahlung terms are not taken into account in any potential scattering model. Electrodynamic corrections of this nature involving strong interactions have not been calculated to our knowledge. In this connection we remark that since the pion form factor effect is at most 10% in the differential cross section, violation of charge symmetry in the strong interaction at a relatively low level would be serious from our point of view. However, in a recent review, Henley[40] sets an upper limit of 0.8% on charge-symmetry violation in hadronic forces; this would correspond to less than 0.05F in the pion radius.

Conclusion

We have measured the elastic differential cross section for $\pi^{\pm} + \alpha \rightarrow \pi^{\pm} + \alpha$ scattering. Several energies have been used and the phase shifts have been evaluated. Several methods and models have been used in an attempt to extract the pion electromagnetic radius. The detailed model available for describing the pion nucleus strong interaction, which also reduces model dependence as much as possible, is the method used in Part B of the analysis. This gives an answer of $R_{\pi} = 2.96 \pm 0.43$ F. However, as shown in Table VI, the result varies from method to method. Further, we have pointed out some inadequacies in the model, particularly in relation to its non-relativisitic nature.

Acknowledgements

With great pleasure I thank Professor Kenneth Crowe for his constant help and encouragement throughout this experiment. Also, I gratefully thank Dr. Anthony S. L. Parsons who participated in the experiment at every phase and whose advice, expertise, and general good humor was invaluable. The work of Dr. Jacques Miller who helped set up the preliminary run, is deeply appreciated.

In any experiment of this sort, there are a multitude of people whose assistance was essential at one point or another. The help of the following in particular, is gratefully acknowledged: Leonard Proehl, who was a great help with the electronics; Norman Gunther, who wrote many of our Monte Carlo and data reduction computer programs surmounting innumerable Mode 4 arithmetic errors; Roger Bell and John Rhodes, who patiently helped at all hours during the run and greatly assisted in the data reduction afterwards; their comments, particularly on the last owl shift, were a constant source of encouragement, lightening the burden of sleeplessness; Michael Wolfson, who wrote the Monte Carlo program, tracing pions and muons from the cyclotron target to our experimental target; Mrs. Patricia Efthimiou, who did and excellent job of typing and interpreted my unspeakable handwriting with uncanny accuracy.

Also, many illuminating conversations with Tom Mottershead, Professor Robert Riddell and Dr. Joel Yellin on the various theoretical methods of interpreting the data are acknowledged with sincere thanks.

Of course, we deeply appreciate the excellent assistance of Jimmy Vale, Lloyd Hauser and the rest of the cyclotron crew, as well as the E. M. crew, and the electronic support group of Building 14.

If I have forgotten others, I ask their forgiveness and assure them that the oversight was unintentional.

Finally, I wish to thank my wife Louise for her understanding and encouragement during these past years.

Appendix

The distortion Amplitude used in Section B we write

$$f^{\pm} = [\Sigma(2\ell+1)(f_\ell^N \pm f_\ell^D \pm f_\ell^{size})P_\ell(\cos\theta)] \pm f^{pt}$$

$$= \Sigma(2\ell+1)\, f_\ell^{\pm}(\cos\theta) \pm f^{pt},$$

where the amplitude f_ℓ^D is defined to be the distortion amplitude in the ℓth partial wave; if the strong interaction vanishes, it disappears. The amplitudes f^{size} arise from the deviation from a point-charge distribution and are purely Coulomb; f^{pt} is the point-charge amplitude,

$$f_\ell^N = \frac{(f_\ell^+ + f_\ell^-)}{2},$$

and

$$\Sigma(2\ell+1)\, f_\ell^{size} P_\ell(\cos\theta) = (F-1)\, f^{pt},$$

where F is the product of the electromagnetic form factors for the helium and the pion. The amplitudes f_ℓ^D are found by solving Eq. (1) with and without strong interactions, using

$$f^D = \frac{(f_\ell^+ - f_\ell^- - f_\ell^{size})}{2}.$$

Although f_ℓ^{size} varies with the charge radius, we find f_ℓ^D to be almost independent of this input, and this small variation in f_ℓ^D is included in assigning its error as are the various sensitivities of f_ℓ^D to changes in each of the optical parameters.

Footnotes and References

*Work done under the auspices of the U. S. Atomic Energy Commission.

†Present address: Centre d'Etudes Nucléaires, Saclay, France.

1. W. Frazer and J. Fulco, Phys. Rev. 115, 1763 (1959); 117, 1609 (1960).

2. M. M. Sternheim and R. Hofstadter, Nuovo Cimento 38, 1854 (1965).

3. M. E. Nordberg, Jr., and K. F. Kinsey, Phys. Letters 20, 692 (1966).

4. L. I. Schiff, Progr. Theor. Phys. Supplement 400 (1965).

5. M. L. Godberger & K. M. Watson, Collision Theory (John Wiley & Sons, New York, 1964), p.203.

6. G. B. West, Phys. Rev. 162, 1677 (1967).

7. E. H. Auerbach, D. M. Fleming, and M. M. Sternheim, Phys. Rev. 162, 1683 (1967).

8. M. M. Block, Phys. Lett. 256, 604 (1967).

9. M. M. Block, I. Kenyon, J. Keren, D. Koetke, P. Malhotra, R. Walker, and H. Winzeler, Phys. Rev. 169, 1074 (1968).

10. S. N. Berman (Stanford University), private communication.

11. D. G. Cassel (Thesis), NP-14885, Princeton, 1965.

12. N. Zagury, Phys. Rev. 145, 1112 (1966).

13. C. W. Akerlof, W. W. Ash, K. Berkelman, C. A. Lichtenstein, A. Ramanauskas, and R. H. Siemann, Phys. Rev. 163, 1482 (1967).

14. C. Mistretta, D. Imrie, J. A. Appel, R. Budnitz, L. Carroll, M. Goitein, K. Hanson, and Richard Wilson, Phys. Rev. Letters 20, 1523 (1968).

15. E. H. Auerbach, D. M. Fleming, and M. M. Sternheim, Brookhaven

Laboratory Report BNL-12309, 1968.

16. W. H. Barkas and A. H. Rosenfeld, Data for Elementary-Particle Physics, UCRL-8030-Rev. Oct. 1, 1961 (unpublished).

17. A. H. Rosenfeld, N. Barash-Schmidt, A. Barbaro-Galtieri, L. R. Price, P. Soding, and C. G. Wohl, Data on Particles and Resonant States UCRL-8030, Rev. Jan. 1968.

18. F. Crawford - UCRL-1753, Jan. 27, 1953, (unpublished).

19. D. H. Stork, Phys. Rev. 93, 868 (1954).

20. H. Byfield, Phys. Rev. 86, 17 (1952).

21. A. Donnachie, R. G. Kirsopp, and C. Lovelace, CERN Report TH-838 1967.

22. D. Bodansky, A. M. Sachs, and J. Steinberger, Phys. Rev. 93, 1367 (1954).

23. L. S. Kisslinger, Phys. Rev. 98, 761 (1955).

24. K. M. Watson, Rev. Mod. Phys. 30, 565 (1958).

25. This modification was derived by C. T. Mottershead.

26. M. L. Goldberger and K. M. Watson, op cit., p.340.

27. For 60 MeV, E_{eq} = 184.7 MeV, compared with $E_{\pi_{c.m.}}$ = 194.2 MeV. if $E_{\pi_{c.m.}}$ is used in the optical-model analysis, and the recoil is neglected, the final answer for the radius of the pion is larger by 10% for this method analysis.

28. H. Frank, D. Haas, and H. Prange, Phys. Letters 19, 391, 719 (1965).

29. G. R. Burleson and H. W. Kendall, Nucl. Phys. 19, 68 (1960).

30. E. Leader, Nucl. Phys. 26, 177 (1961).

31. M. M. Sternheim, Phys. Rev. 98, 761 (1955).

32. W. F. Baker, J. Rainwater and R. E. Williams, Phys. Rev. 112, 1763 (1958), R. M. Edelstein, W. F. Baker, and J. Rainwater, ibid 122 252 (1961).

33. E. T. Whittaker and G. N. Watson, Modern Analysis (Macmillan Company, New York, 1947), p. 197-201.

34. C. T. Mottershead (Lawrence Radiation Laboratory), private communication.

35. Dr. Joel Yellin is herewith thanked for enlightening conversations on this question, which is being further investigated by him and by Ron Christensen.

36. P. Auvil, Phys. Rev. 168, 1568 (1968).

37. P. Thurnauer, Proceedings of the New York Meeting of the American Physical Society (1969).

38. M. Ericson, Nuovo Cimento 47, 49 (1967).

39. J. Rix and R. M. Thaler, Phys. Rev. 152, 1357 (1966).

40. Henley, Nuclear Forces, to be published in Isospin in Nuclear Physics.

Figure Captions

Fig. 1. Layout of the pion beam line.

Fig. 2. Range curve for π^- obtained in the scattered beam (data from 70 and 75 deg. combined).

Fig. 3. The basic elements of the logic set-up. F BIN 3 is shown in detail. F BIN 4 mixes telescopes 2, 8, 13, F BIN 5 mixes 3, 19, 14, etc.

Fig. 4. Pulse-height spectra obtained in the scattered beam at 70 deg. for (a) 51-MeV π^+, (b) 60-MeV π^+, (c) 75-MeV π^+, (d) 60-MeV π^-. Empty target background has been subtracted. Typical error bars are shown. The solid curves are the best fit of two Gaussian curves to the experimental distribution.

Fig. 5. A Gaussian fit to the pulse height distribution of a counter in the beam.

Fig. 6. a) Parameters used in measuring a solid angle subtended by a rectangle.

b) Geometry used in solid angle correction.

Fig. 7. Elastic differential cross sections for πp at 60 MeV for (a) π^+. (b) π^-. The solid curves are the differential cross sections from the phase shifts of Ref. 15.

Fig. 8. Cross sections for (a) π^+ and (b) π^- at 60 MeV with best phase-shift fits, and (c) average cross section with best optical-model fit.

Fig. 9. D/A as a function of cos $\theta_{c.m.}$, with best optical-model fits. for (a) 51 MeV, (b) 60 MeV (c) MeV (d) 75 MeV.

Fig. 10. Optical parameters - Reb_o and Reb_1 for this and other experiments with theoretical curve. Spread indicates uncertainty in the latter.

Fig. 11. Optical parameter Imb, with theoretical curve and spread.

Fig. 12. The quantities -A and B are plotted vs cos $\theta_{c.m.}$ for 60 MeV (see Eq. 2). The data points represent -A. The shaded area represents B with its uncertainty.

Fig. 13. (a) F_π plotted vs q^2. Best-fit curve is shown together with displacements of data points caused by shifting relative $\pi^+ - \pi^-$ normalization by its error.

(b) R_π vs q^2 for both extrema of the relative normalization. Two points at the largest value of q^2 are missing because they are not real. The best-fit value and error are plotted for reference.

Fig. 14. Feynman diagrams not taken into account by the optical model.

TECHNICAL INFORMATION DIVISION
LAWRENCE RADIATION LABORATORY
UNIVERSITY OF CALIFORNIA
BERKELEY, CALIFORNIA 94720